1

2

3

4 **Extrinsic repair of injured dendrites as**

5 **a paradigm for regeneration by fusion**

6

7

8

9

10

11

12 Meital Oren-Suissa[1,2], Tamar Gattegno[1], Veronika Kravtsov[1], and Benjamin

13 Podbilewicz[1†]

14

15 [1] Department of Biology, Technion- Israel Institute of Technology, Haifa 32000,

16 Israel

17 [†] Author for correspondence (podbilew@tx.technion.ac.il)

18 Additional footnotes:

19 [2] Present address: Howard Hughes Medical Institute, Columbia University, Department of

20 Dept. of Biological Sciences, New York, 10027, USA

21

22

23

24

1

## Highlights

- New system to study dendritic plasticity, regeneration and degeneration

- Following dendrotomy AFF-1 is activated to bypass the lesion via auto-fusion

- Extracellular AFF-1-vesicles derived from the epidermis fuse severed neurons

- EFF-1 prunes injury-induced ectopic sprouting

- Combined activities of the fusogens EFF-1 and AFF-1 regenerate arbors

## Abstract

Injury triggers regeneration of axons and dendrites. Research identified factors required for axonal regeneration outside the CNS, but little is known about regeneration triggered by dendrotomy. To determine how neurons regenerate dendrites following injury we study the *C. elegans* PVD polymodal neurons that display an arborized pattern of repetitive menorah-like structures. We injure dendrites by laser microsurgery, follow their fate and show that broken primary dendrites often regenerate via fusion. We describe how PVD dendrites regenerate and present roles for EFF-1 and AFF-1 glycoproteins in fusion and remodeling of menorahs. Menorahs lose self-avoidance and AFF-1 fuses them, bypassing the injury site. Branch sprouting, EFF-1-mediated pruning, and arbor simplification completes regeneration. When auto-fusion fails the distal arbor degenerates. Surprisingly, AFF-1 acts non-cell autonomously to mediate dendrite fusion. We propose that extracellular vesicles derived from the lateral epidermis fuse severed dendrites in a process reminiscent of enveloped virus-mediated cell fusion without infection.

48

## Introduction

50    Sensory perception relies on networks of neurons that monitor and modify behavior to

51    assure that animals are able to locate food, sense their environment and avoid

52    predators or other threats [1]. This perception depends on the integrity and spatial-

53    coverage of the receptive field [2]. Axonal and dendritic trees play an essential role in

54    processing and transducing information to ultimately evoke the appropriate response

55    of the organism. In the central nervous system (CNS) of adult mammals axon

56    regeneration following injury is limited [3]. Therefore, the regenerative process

57    following axon severing has been the focus of numerous studies [3-5]. It is believed that

58    the main reasons why axons fail to regenerate are a reduction in neuronal growth

59    capacity and inhibitory extrinsic factors. However, the molecular mechanisms of

60    regeneration are not well understood. Recent studies have suggested that modulation

61    of intrinsic neuronal activity by mammalian target of rapamycin (mTOR) and G-

62    protein-coupled receptor (GPCR) signaling promote axon regeneration [4,6]. In parallel

63    there is evidence for a molecular pathway for axonal degeneration that affects

64    regeneration [7]. The molecular mechanisms required for regeneration by regrowth

65    following axonal injury are actively studied and numerous pathways have been

66    identified [3-5,8-12]. In contrast to regeneration by regrowth, a different strategy for

67    axonal regeneration that has been observed in diverse invertebrates is reconnection by

68    fusion of severed axons [13-18].

69         The nematode *C. elegans* is a powerful model to study neuronal regeneration

70    after injury. It has been recently found that injured axons of motor- and

71    mechanosensory-neurons regrow and in some cases fuse after *in vivo* severing using

3

72    laser surgery [15,16,18-20]. Moreover, screens for genes with roles in axon regrowth

73    identified many genes required for axon regeneration [15,21,22].

74         Compared to axonal regeneration and degeneration pathways, much less is

75    known about dendritic regeneration following injury [23-27]. Recent studies have

76    identified the PVD and FLP neurons as highly branched bilateral neurons in *C.*

77    *elegans,* which display a stereotypic arborization pattern composed of repetitive

78    structural units known as menorahs (**Figures 1A and 1B**)[28-36]. The PVD is highly

79    polarized with a single axon ventral to the cell body and a complex but stereotyped

80    dendritic arbors [32,36] making it an ideal system to study different aspects of the

81    generation, maintenance, regeneration and degeneration of dendritic trees. The PVD

82    neurons are two polymodal nociceptors, responsible for an avoidance response

83    generated after harsh mechanical stimuli to the main body or exposure to cold

84    temperatures [1,37,38]. Animals in which PVD neurons are laser-ablated fail to respond to

85    harsh touch [37]. Recent studies uncovered the degenerin ion channels DEG/ENaC,

86    MEC-10 and DEGT-1 that sense harsh-touch, and the TRPA-1 channels that respond

87    to cold temperatures [34,39]. Moreover, researchers have identified numerous genetic

88    pathways involved in dendritic arborization and maintenance of the PVD structure

89    [32,40-46].

90         The dynamic pathway of PVD arborization revealed an unexpected function of

91    EFF-1 fusogenic protein in sculpting neuronal trees [32]. EFF-1 mediates epithelial and

92    muscle cell-to-cell fusion [47-52], auto cell fusion in the digestive tract [53], axonal fusion

93    following injury [15,17,18,20] and acts in the PVD neurons to trim menorahs [32]. *eff-1*

94    mutants have hyperbranched disorganized menorahs and EFF-1 cell-autonomous

95    expression is sufficient to reduce the number of branches and to rescue disorganized

96    menorahs [32]. EFF-1 controls dendritic plasticity via retraction of excess branches, by

97    fusing branches and by forming loops that restrict further growth [32]. AFF-1, a paralog

98    of EFF-1, mediates fusion of the anchor cell to form the utse/hymen, fuses the lateral

99    epidermal seam cells and merges some embryonic epithelial cells [54]. In addition, AFF-

100   1 is induced by Notch to auto-fuse a myoepithelial toroid [53], and fuses the excretory

101   duct cell to form a single-cell tube [55].

102       Here we studied neuronal plasticity triggered by dendrotomy and determined

103   the fate of complex PVD arbors following laser surgery of dendrites. We found that

104   severed primary dendrites grew towards each other and reconnected via branch

105   fusion. Simultaneously, terminal branches lost self-avoidance and grew towards each

106   other, meeting and fusing at the tips via an AFF-1-mediated process. Ectopic branch

107   growth was identified as a step in the regeneration process required for bypassing the

108   lesion site. Failure of reconnection to the severed dendrites resulted in degeneration of

109   the distal end of the neuron. We discovered pruning of excess branches via EFF-1 that

110   acted to recover the original wild-type arborization pattern in a cell-autonomous

111   process. In contrast, AFF-1 activity during dendritic auto-fusion was derived from the

112   lateral seam cells and not autonomously from the PVD neuron. We propose a model

113   in which AFF-1-vesicles derived from the epidermal seam cells fuse neuronal

114   dendrites from without. Thus, EFF-1 and AFF-1 fusion proteins emerge as new

115   players in neuronal arborization and maintenance of arbor connectivity following

116   injury in *C. elegans*. Our results demonstrate that there is a genetically determined

117   multi-step pathway to repair broken dendrites in which EFF-1 and AFF-1 act on

118   different steps of the pathway. Intrinsic EFF-1 is essential for dendritic pruning after

119   injury and extrinsic AFF-1 is transported in vesicular carriers to mediate dendrite

120   fusion and to bypass injuries.

121

122 ## Results

123 **Dissection of dendritic regeneration in *C. elegans* mechanosensory neurons**

124 The regenerative ability of axons following injury has been previously described in

125 vertebrates and invertebrates [14,56-59]. The morphological and molecular changes that

126 occur following dendritic amputation remain mostly unexplored [23-26,32,60,61]. To study

127 the process of regeneration of the PVD dendrites following amputation we performed

128 dendrotomy of arborized neurites using a femtosecond laser [8,15,16,19]. A successful

129 regeneration was defined as a process in which the severed branch was able to

130 reconnect with its target [62]. Failure to rejoin the two parts of the severed primary

131 dendrite results in degeneration of the distal part and in some cases a complete

132 degeneration without regrowth of the multi-menorah dendritic tree. Temporal analysis

133 of PVD dendrite dynamics following injury revealed several overlapping steps in

134 arbor regeneration (**Figure 1C**). PVD dendrites showed robust regeneration when

135 severed at the L4 stage. We found that severed primary dendrites grew towards each

136 other (**Movies 1 and 2**) and in around 40% of the animals were able to reconnect the

137 distal end to the soma via fusion (**Figure 1D and 1E**).

138 It was shown that following axotomy of the PLM mechanosensory neuron,

139 reconnection of the axon to the distal branch is dependent upon EFF-1, but not AFF-1

140 activity [17,18,20]. In contrast, we found that primary dendrotomies in *eff-1* or *aff-1* single

141 null mutants were repaired and regeneration via primary branch fusion occurred

142 (**Figure 1F**). Due to the sub-viability of *eff-1aff-1* double mutants [54], we were unable

143 to test whether there is redundancy between these genes in primary branch fusion. It is

144 conceivable that there is redundancy in the fusion machinery that fixes broken

145 neurites or that an unidentified fusogen is required for postembryonic primary

146 dendrite auto-fusion after microsurgery. Failure to reconnect following dendrotomy

6

147   resulted in degeneration of the distal end and took place within 12 hr in about 20% of

148   the operated animals (**Figure 1G**, arrow, **1H** and **Movie 3**). Thus, following primary

149   branch microsurgery the two ends grow towards each other, the tips meet, connect

150   and the integrity of the distal arbors is maintained.

151   **Dendrotomy reveals menorah plasticity and causes loss of self-avoidance**

152   The dendritic architecture of the PVDs is maintained by a contact-dependent self-

153   avoidance mechanism. The tertiary branches withdraw upon contact of a neighboring

154   branch, maintaining the menorah architecture [33,42]. To test whether self-avoidance is

155   maintained after injury, we explored the spatial dynamics of regenerating dendrites.

156   Two hours after injury, we observed tertiary branches from neighboring menorahs

157   that contacted each other and extended far from their initial location, resulting in a

158   structure of overlapping menorahs throughout the neuron (**Figure 1D and 1E**,

159   bracket). Some of these overlaps extended and occurred between menorahs

160   originating from both sides of the lesion (**Figure 1-figure supplement 1 brackets**

161   **and Movies 1 and 2**). These overlapping structures persisted even 48 hr after the

162   injury (**Figure 1-figure supplement 1F**). Dendrotomy at earlier stages, such as the L3

163   stage, showed similar results; animals exhibited loss of avoidance-mechanisms and

164   branch overlap (data not shown). These results suggest that upon injury the avoidance

165   mechanisms are lost, making it more likely that a new connection will form to

166   compensate for the injury.

167   **Menorah-menorah fusion bypasses the severed primary dendrites**

168   We have previously shown that during wild type development PVD and FLP terminal

169   quaternary branches can auto-fuse with one another to maintain menorah structure

170   and to limit further growth [32]. To determine whether fusion of terminal dendrites is

171   part of the regeneration process, we analyzed the overlapping branches after injury

7

172   and found that most of the reconnections bypassed the injury site through menorah-

173   menorah fusion, resulting in giant menorahs (**Figures 2A-2D, and Figure 2- figure**

174   **supplement 1B,** brackets). To judge the connectivity of the tertiary branches we

175   verified that the distal processes do not degenerate, and analyzed GFP-signal

176   continuity using confocal microscopy and live imaging (**Figure 2D**, **Movies 1, 2 and**

177   **4**). In addition we used a photoactivatable Kaede cytoplasmic reporter expressed in

178   the PVD to demonstrate that the menorahs have fused and therefore have connected to

179   bypass the lesion site (**Figure 2- figure supplement 2**). We found that in animals

180   where menorah-menorah fusion took place the distal fragment did not degenerate,

181   regardless of primary-primary branch reconnection (n=23). Thus, terminal branch

182   auto-fusion acts as a mechanism to bridge the gap between the PVD soma and the

183   distal end to maintain connectivity and avoid degeneration.

184   **Sprouting, pruning, and arbor simplification complete regeneration**

185   We observed that the PVD dendrites appeared highly dynamic after injury, showing

186   ectopic growth of terminal branches. These results suggested that growth is not

187   restricted to a subset of branches, and can occur throughout the neuron, allowing for

188   massive regeneration (**Figures 2C and S1**; asterisks). To verify that growth is

189   stimulated specifically due to the dendrite injury and not because of laser damage, we

190   examined mock-injured animals for PVD morphology changes. We injured animals

191   near the PVDs, at the same focal plane, but without hitting any dendrite. PVD mock-

192   operated animals showed normal growth with no excess sprouting or changes in the

193   PVD morphology (data not shown). These results demonstrate that dendrite severing

194   specifically induced terminal branch reconnection by fusion, ectopic sprouting and

195   regeneration (**Figure 1C**, **Movies 1 and 2**).

196       Interestingly, some of the distal secondary stems were eliminated following

197    the reconnection, leaving just one or two secondary stems per giant menorah (**Figures**

198    **2C and Figure 2- figure supplement 1B**; arrows). These dendritic rearrangements

199    persisted even 48 hr after surgery, leading to simplification of the dendritic trees and

200    leaving mainly giant menorahs. Thus, active elimination of excess branches occurs in

201    order to recreate a pattern resembling wild-type menorahs. Analysis of time-lapse

202    movies showed that excess branches were eliminated, and pruning occurred

203    concomitantly with growth around the injury site (**Figure 2D** and **Movie 4**). Taken

204    together, the PVD dendrites are able to successfully regenerate following dendrotomy,

205    inducing dynamic remodeling by branch growth and elimination (**Figure 1C**).

206    **EFF-1 is essential for pruning excess branches after dendrotomy**

207    The central function of EFF-1 in PVD developmental arborization is in quality control

208    trimming of excess and abnormal branches [32]. To determine whether EFF-1 acts in

209    simplification following injury we amputated primary dendrites in *eff-1* mutants and

210    followed the repair process. We found that *eff-1* mutants maintained hyperbranched

211    and disorganized menorahs and failed to simplify the dendritic tree following injury

212    (**Figure 2E**). These phenotypes suggest that *eff-1* acts in branch retraction and

213    simplification induced by severing of the primary branch. We were not able to

214    determine whether *eff-1* participates in menorah-menorah fusion because the

215    hyperbranched and severely disorganized arbors prevented us from identifying

216    menorah fusion and additional ectopic sprouting (**Figure 2F**). In contrast, both uncut

217    and dendrotomized *eff-1* mutants showed no pruning, demonstrating that *eff-1* is

218    required for branch simplification following dendrotomy. In addition, cell-

219    autonomous expression of EFF-1 in the PVD resulted in excess pruning. Thus, EFF-1

220    acts cell autonomously to simplify excess sprouting following dendrotomy and is

221    sufficient to trim branches and simplify arbors.

222    **AFF-1 is required to bypass cut dendrites via menorah-menorah fusion**

223    Since the *C. elegans* known fusogens, EFF-1 and AFF-1, are essential and sufficient

224    to fuse cells in *C. elegans* and heterologous cells in culture [49,50,54,63,64], we

225    hypothesized that they may be required to regenerate broken neurites by homotypic

226    fusion.

227         Because EFF-1 prunes dendrites by branch retraction we decided to determine

228    a possible role for *aff-1* following dendrotomy, we asked whether menorah-menorah

229    fusion occurs in *aff-1* injured-mutants. We found that while in *aff-1* mutants dendrite

230    development was normal (**Figure 3A**), following dendrotomy most of the

231    reconnections were between the re-growing primary dendrite and its distal fragment,

232    rather than through menorah fusion as in wild-type animals (**Figure 3D**). This

233    observation suggests a fusogenic function for AFF-1 in terminal branch fusion. In *aff-*

234    *1* mutant animals we found some exceptions in which some menorahs overlapped, but

235    we did not observe fusion between menorahs followed by secondary stem

236    degeneration (**Fig. 3D**). In dendrotomized *aff-1* animals failure to rejoin the dendritic

237    trees resulted in degeneration of the distal part of the arbor (**Figs. 3A and 3D**). Thus,

238    while *aff-1* has no apparent role in normal PVD arborization, it is required for

239    terminal branch fusion following dendrotomy.

240         AFF-1-mediated membrane fusion of terminal branches emerges as the main

241    mechanism by which dendritic repair occurs in *C. elegans*. We were not able to detect

242    *aff-1* expression in the PVD neither before nor after dendrotomy. To determine

243    whether AFF-1 acts extrinsically to the PVD to reconnect dendrites we attempted to

244    rescue menorah-menorah fusion in *aff-1* mutant using expression of *grd-10p*::AFF-1

10

245  in the epidermal seam cells. We found induced recovery of reconnection and reduced

246  degeneration to wild-type levels (**Figure 3B-3D**). In contrast, we found that PVD

247  expressing *des-2p*::AFF-1 was not able to rescue the menorah-menorah fusion failure

248  phenotype (**Figure 3D**). Expression of *dpy-7p::aff-1* from the hypodermis was toxic

249  in *aff-1* homozygous mutants but improved PVD regeneration in heterozygous *aff-1/+*

250  animals, suggesting that non-autonomous expression from the surrounding

251  hypodermis is also sufficient to improve the ability of the PVD to rejoin the branches

252  by fusion (**Figure 3-figure supplement 1**). The non-cell autonomous activity of AFF-

253  1 in PVD regeneration by auto-fusion was unexpected since for cell-cell fusion AFF-1

254  acts homotypically in both fusing plasma membranes [64].

255  **AFF-1-containing extracellular vesicles repair the PVD by fusing with it**

256  To determine AFF-1 expression and localization before and after dendrotomy we

257  imaged AFF-1::GFP in worms expressing mCherry in the PVD. We could not detect

258  AFF-1 in the PVD at any stage during development or following dendrotomy. Instead,

259  AFF-1 is strongly expressed on the plasma membrane, filopodia and internal puncta

260  in the lateral seam cells. This was expected since the seam cells fuse homotypically

261  between the L4 and adult molt via AFF-1-mediated fusion [54]. Using structured

262  illumination microscopy we found extracellular puncta containing AFF-1::GFP that

263  apparently were derived from the seam cells. (**Figure 4A,** arrowheads). Using live

264  spinning disk confocal microscopy we found that the vesicles containing AFF-1::GFP

265  were observed outside the seam cells in control animals that were not dendrotomized

266  (**Figure 4B, Movies 5, 6 and 9**). Following dendrotomy the AFF-1::GFP signal in the

267  seam cells was brighter (**Figure 4C**) and there was a five-fold increase in the mobility

268  and number of extracellular vesicles (**Figure 4D-4F, Movies 7, 8, 10 and 11**). Thus,

11

269    taken together our results show that AFF-1 regenerates severed PVD dendrites in a

270    surprisingly non-cell autonomous way from the seam cells.

271

272    **Discussion**

273    **AFF-1-extracellular vesicles merge injured neurons from without**

274    Cell-cell fusion from within occurs when a fusogenic protein (e.g. a viral fusion

275    protein following infection) or an endogenous cellular fusion protein (e.g. EFF-1) is

276    expressed intrinsically in cellular compartments, including the plasma membrane.

277    Fusion from without occurs when a viral particle fuses target cells without infecting

278    them [65-67]. Here we discovered an example of fusion from without during neuronal

279    regeneration.  We propose that epidermal seam cells shed extracellular vesicles that

280    travel 1000 nm or less to reach the PVD severed dendrites and the menorahs. These

281    vesicles contain AFF-1 and can fuse dendrites from without (**Figure 5**). AFF-1-

282    containing vesicles derived from the lateral epidermal seam cells mediate fusion of

283    severed dendrites and menorah auto-fusion to bypass the injury and to maintain

284    dendritic tree structure and function. Extracellular vesicles (EVs, microvesicles,

285    exosomes and ectosomes) from different sub-cellular and tissue origins have been

286    proposed as vehicles for cell-cell communication during normal physiology,

287    participate in the immune response, control coagulation and promote metastatic

288    cancer [68]. These extracellular vesicles have been shown to exist in bacteria, archea,

289    plants, fungi and animals [69-73]. In *C. elegans* EVs derived from ciliated neurons affect

290    mating behavior and communication between animals [74]. Signaling EVs derived from

291    the sperm activate oogenesis and ovarian muscle contraction [75]. EVs also participate

292    in engulfment of dead cells [76] and morphogenesis of the embryo [77].

12

293      EVs are probably universal but diverge in size, shape and place of origin.

294    They contain lipid bilayers, transmembrane proteins and nucleic acids. One of the

295    characteristics of these EVs is their ability to fuse to target cells and deliver RNAs,

296    plasmids, toxins and signaling molecules. However, the fusion proteins necessary to

297    deliver and merge the diverse EVs have not been identified and characterized in any

298    system. Mammalian cells transfected with *C. elegans* AFF-1 produce extracellular

299    vesicles that have been biochemically and ultrastructurally characterized [64,78].

300    Moreover, AFF-1-containing vesicles and pseudotyped particles are able to fuse to

301    mammalian cells expressing EFF-1 or AFF-1. Thus, AFF-1 can mediate fusion of

302    extracellular vesicles to cells expressing EFF-1 on the plasma membrane in a tissue

303    culture system [64,78]. Here we provide the initial evidence for a mechanism that can

304    fuse EVs to target neuronal cells in vivo. Surprisingly, these EVs can cause auto-

305    fusion from without mediated by AFF-1 transmembrane fusion protein on their

306    surface. Moreover, these AFF-1-EVs derived from the *C. elegans* lateral epithelia can

307    fuse neurons in vivo, thus directly promoting regeneration (**Figure 5**).

308    **Neurodevelopmental genetic stages in dendrite repair after injury**

309    The primary mechanism of PVD dendritic regeneration can be divided into five

310    stages: (1) reattachment at site of injury, (2) loss of self-avoidance between adjacent

311    menorahs, (3) menorah-menorah fusion to bypass lesions, (4) sprouting of

312    compensatory branches and (5) pruning of excess branches (**Figure 1C**).

313      The interplay between two effector fusogens revealed a genetic pathway that

314    links membrane remodeling during normal development and following neuronal

315    injury. Here we focused on two cellular stages: Extrinsic stage (3) AFF-1-mediated

316    menorah-menorah fusion from without and intrinsic stage (5) EFF-1-mediated

317    trimming of excess branches from within. (**Figures 1C** and **5**).

318 **AFF-1 merges terminal branches to bypass broken dendrites**

319 Axonal fusion after injury is crucial for reestablishing synaptic contacts, to prevent

320 degeneration, and for regaining neurological functionality [62]. Although *eff-1* mutants

321 failed to fuse broken axons [20], *eff-1* mutants succeed to merge injured dendrites. We

322 tested the two known *C. elegans* fusogens, EFF-1 and AFF-1, as well as the EFF-1

323 paralog, C26D10.7 ([50,79] and Oren-Suissa and Podbilewicz, unpublished results). We

324 found that terminal-branch fusion following dendrotomy was significantly reduced in

325 *aff-1* mutants compared to wild-type. However, none of these genes was

326 independently required for primary dendrite fusion following an injury, suggesting

327 either redundancy or that yet another *C. elegans* fusogen awaits identification. Based

328 on these observations, we conclude that *aff-1* is required to heal dendritic wounds,

329 specifically via menorah-menorah fusion.

330     Our data support a model in which *aff-1* and *eff-1* expression is highly

331 regulated in the PVD. Following dendrotomy *eff-1* expression appears to be repressed

332 allowing ectopic sprouting of terminal branches and loss of self-avoidance

333 culminating with AFF-1-mediated menorah-menorah fusion via a surprising non-

334 autonomous mechanism of fusion from without (**Figure 5**).

335 **EFF-1 retracts and simplifies excessive branching following injury**

336 The development of the nervous system includes the formation of many new

337 branches, yet some of them are later eliminated. This process is termed pruning and is

338 crucial for the formation of stable connections. [80-85]. In the central and peripheral

339 nervous systems, axons that are severed from their cell bodies degenerate by the

340 genetically active process of Wallerian degeneration (WD) [7]. WldS mutant mice

341 present slow WD and the persistent axon fragments appear to prevent regeneration by

342 regrowth [7]. In addition, the ubiquitin/proteasome system acts to regulate axon

14

343 degeneration in Drosophila, in vitro and in mice [86]. Thus, failure to remove axon

344 debris following injury may physically block regeneration by regrowth of severed

345 axons and WD appears to be required for efficient regeneration by regrowth [87].

346 Developmental pruning occurs in *C. elegans* AIM interneurons, and this process is

347 regulated by the helix-turn-helix transcription factor MBR-1 [88] and Wnt-Ror kinase

348 signaling [81]. Here, we demonstrated a novel mechanism of branch pruning following

349 injury. We have previously shown that significant refinement is required to maintain

350 the complex web of dendrites in the final state of perfectly sculpted PVD menorahs [32].

351 This dynamic nature persists following dendrotomy, and many new branches sprout

352 around the injury site to ensure a successful connection will occur. This burst of

353 growth is followed by the elimination of excess branches, and the arbor is simplified

354 to resemble the original tree. This process is normally repressed probably by

355 transcriptional mechanisms. Following injury and a stimulation of ectopic branching,

356 *eff-1* is activated to simplify the arbors and regenerate a normal structure of menorahs.

357 These results suggest that there is conservation of the molecular machinery for neurite

358 refinement, and that the ability to alter existing morphologies is a key component in

359 the development and survival of nervous systems.

360 **Is auto-fusion an alternative pathway to repair severed neurons?**

361 Fusion of severed axons occurs in invertebrates for example in Aplysia [13], crayfish[14]

362 and *C. elegans* [15-18] but rarely in vertebrates [6,89]. Why is this the case and how can our

363 study help us understand this? Invertebrates and vertebrates do have conserved

364 pathways to regenerate injured branches via regrowth [3,4,9,15,90-92]. However, it appears

365 that fusion of broken neurites or bypassing the injured site using fusion instead of

366 rebuilding complex trees is a more energetically economical process. The use of

367 extracellular vesicles could be a useful strategy to stimulate repair of injured branches

15

368    in the CNS of vertebrates that usually cannot regenerate.

369    **Severed neurites can reconnect by suspending self-repulsion mechanisms**

370    We have found that in *C. elegans* PVD, following dendrotomy there is a transient loss

371    of self-avoidance between the menorahs (tertiary branches) that allows the

372    reconnection by merging the menorahs and bypassing the site of injury, thus

373    maintaining the dendritic trees. This is consistent with studies in leech embryos

374    showing that laser microbeam severing of neurites of mechanosensory neurons result

375    in that the detached branch stopped being avoided by the rest of the cell. This is

376    consistent with a mechanism that controls self-avoidance and that requires physical

377    continuity between the neurites [93]. In *C. elegans* this mechanism appears to involve

378    netrins [42]. In contrast, in zebrafish detached fragments continue to repel the parent

379    arbor [87]. Thus in zebrafish and probably in other vertebrates it is required to have a

380    WD-like mechanism to remove fragments of sensory neurites before the process of

381    regrowth can occur. It would be useful to find ways to induce merging of the severed

382    neurites as occurs in some invertebrates.

383          Spinal cord injuries, experimental axotomies, surgical accidents, and diverse

384    forms of neurodegeneration are all conditions that currently cannot be generally

385    repaired [3,6,58,59,94]. Unveiling the mechanism of intrinsic *eff-1*-mediated dendritic

386    simplification and extrinsic *aff-1*-mediated neuronal auto-fusion from without may

387    pave the way for overcoming neurodegenerative diseases or injuries. The dynamic

388    dendritic plasticity of the PVD neurons and the power of genetics in *C. elegans* along

389    with its amenability for RNAi-based analysis and genome editing will uncover

390    genetic pathways that will enable the study of additional mechanisms involved in

391    PVD arborization during development and following injuries. In *C. elegans* AFF-1-

16

392 containing vesicles derived from epithelia appear to fuse dendrites emerging as a

393 potential effector that could repair broken neurons in heterologous systems.

## Acknowledgements

403

## Materials and Methods

### Strains and transgenic animals

406 All nematode strains were maintained according to standard protocols [95,96]. In addition

407 to the wild-type strain N2, the following mutations, transgenes and strains were used:

408 BP601 *aff-1(tm2214)/mIn1[dpy-10(e128) mIs14] II* [54], MF190 *hmIs4[DES-2::GFP,*

409 *pRF4],* BP328 *eff-1(ok1021) II; hmIs4,* BP450 *hyEx30[myo-2::gfp, DES-2::GFP,*

410 *KS],* BP431 *eff-1(hy21) II; hmIs4* [32], NC1841 (*wdIs52, F49H12.4::gfp*; *rwIs1*, *pmec-*

411 *7::*RFP) [33], CHB392 *[hmnEx133(ser-2prom3::kaede)],* kindly provided by Candice

412 Yip and Max Heiman [97]. Germline transformation was performed using standard

413 protocols [98]. The KS bluescript plasmid was used as carrier DNA. Transgenic lines

414 include: BP709 *[hmnIs133 (ser-2prom3::kaede)], BP1014 aff-1/mln1;*

415 *dzIs53[pF49H12.4::mCherry]Is* was created by crossing *aff-1/ mln1* with

416 *pF49H12.4::mCherry* (kindly provided by Salzburg Y.). BP1015 *aff-1/mln1;*

417     *hmnIs133[ser-2prom3::kaede]; hyEx66 [KS , pCFJ90 (myo-2::mcherry), pME4(des-*

418     *2::AFF-1)].* BP1017 *aff-1/mln1; hmnIs133[ser-2prom3::kaede]; hyEx350[KS*

419     *,pCFJ90 myo-2::mcherry, pTG5 dpy-7p::aff-1],* BP1052 *aff-1/mln1; hmnIs133[ser-*

420     *2prom3::kaede]; hyEx355[KS, pCFJ90 myo-2::mcherry, pTG4 grd-10p::aff-1],*

421     BP1055 *dzIs53[F49H12.4p::mCherry]; hyEx66[pRF4, AFF-1fosmid::GFP, KS],*

422     BP1056 *dzIs53[F49H12.4p::mCherry]; hyEx68[pRF4, AFF-1 fosmid::GFP, KS].*

423     **Molecular Biology**

424     We used RF cloning to insert the *grd-10* promoter upstream to the *aff-1* gene [99], and

425     Gateway cloning [100] to clone *aff-1* into a plasmid containing the *dpy-7* promoter

426     fragment (pDest Dpy7 and pDONR™221). Phusion Hot Start II High-Fidelity DNA

427     polymerase (Thermo Scientific, Waltham, MA) was used to facilitate the cloning

428     process.

429     **Confocal microscopy and live imaging *of C. elegans***

430     Nematodes were mounted on 3% agar pads mixed with 10 mM $NaN_3$ in M9 buffer.

431     For time-lapse analysis, worms were anesthetized with 0.1% tricaine and 0.01%

432     tetramisol in M9 solution [101-103]. Animals were analyzed by Nomarski optics and

433     fluorescence microscopy, using Zeiss LSM 510 META confocal, the Zeiss LSM 700

434     confocal or Nikon eclipse Ti inverted microscope equipped with Yokogawa CSU-X1

435     spinning disk (Yokogawa, Tokyo, Japan) and a sCMOS (Andor, Belfast, UK) camera.

436     Z-stacks were taken with PlanApochromat 60x oil NA=1.4 objective using the SDC

437     or 63x NA=1.4 objective using the LSM. When using the sCMOS (Andor) camera z-

438     stacks were taken with ~0.35 μm z-step. When the LSM 510 meta was used, z-step

439     was ~0.8 μm. Image acquisition was done using Andor iQ or Metamorph software

440     (Molecular Devices, Sunnyvale, CA) when using the spinning disk confocal (SDC),

441     and Zen software when using the LSM 510 meta microscope or Zeiss LSM 700.

442    Multidimensional data was reconstructed as projections using the ImageJ and

443    Metamorph softwares. Figures were prepared using ImageJ, Adobe Photoshop CS5

444    and Adobe Illustrator CS6.

445    **Quantifying PVD branching phenotypes and statistics**

446    Quantification was done as previously described [32]. Using confocal microscopy, at

447    least five sequential z-series pictures were taken from each worm. Each z-section was

448    analyzed separately. The results from each worm were normalized to a longitudinal

449    length of 100 μm in all relevant experiments. Significant differences between mutants

450    and wild-type were determined by the two-tailed unpaired t-test, the nonparametric

451    Mann-Whitney test or Fischer's exact test. For each group we observed >20 additional

452    animals that were not recorded by z series on the confocal microscope and that

453    showed similar phenotypes.

454    **Laser surgery**

455    Microsurgery was done using the LSM 510 META and a tunable multiphoton

456    Chameleon Ultra Ti-Sapphire laser system (Coherent, Santa Clara, CA), that produces

457    200-fs short pulses with a repetition rate of 113 MHz and 5 nJ energy at a wavelength

458    of 820 nm. 0.5-2 $\mu m^2$ selected rectangular ROIs of GFP-labeled PVD neurons were

459    cut and successful surgery was confirmed by visualizing targets immediately after

460    exposure. We evaluated the ability of severed neurons to reconnect by analyzing z-

461    stack images of GFP-labeled branches. Dendrotomy was performed on the primary

462    longitudinal process, and the morphological changes were followed for 2 to 72 hours

463    after the surgery. Imaging before and after surgery was done as described above,

464    using the 488 nm line of the Argon laser of the LSM microscope or using the spinning

465    disk confocal system. After surgery, animals were recovered to an agar plate and

466    remounted 5-72 hours after surgery. Recovered worms were analyzed for

19

467    regeneration, fusion between processes, and ectopic sprouting. At least 10 individuals

468    were observed for each experiment. For all worms the primary dendrite was injured

469    anterior to cell body.  Animals were imaged and a z-stack was collected immediately

470    after injury to confirm a successful injury.

471    **Photoactivation using Kaede**

472    In order to verify that dendrites fuse as response to injury we used the

473    photoconvertible protein Kaede driven by a PVD specific promoter *ser-2prom3* [97].  A

474    PVD primary dendrite of *ser-2prom3::Kaede* expressing animals was dendrotomized,

475    animals were recovered for 23 hours and the dendrite reconnection to its stump was

476    assessed by Kaede photoconversion (Kravtsov et al., in revision). The green Kaede

477    form in the PVD cell body was irreversibly photoconverted to the red Kaede form

478    using a 405 nm laser with the Mosaic system (Andor) on the Nikon eclipse Ti

479    inverted microscope. Following photoconversion of the Kaede in the cell body we

480    followed spreading to the dendritic branches for 1 and 60 min post photoconversion.

481    Red Kaede form, though diluted while spreading through the dendritic tree, can be

482    observed beyond the reconnection site of injury in the distal part of the primary and

483    higher ordered dendritic branches. When the dendrites fail to reconnect or

484    immediately after dendrotomy the photoconverted Kaede did not cross the site of

485    injury, revealing that spreading of red Kaede is a reliable tool to confirm rejoining of

486    severed dendrites.

487

488    **References**

489    1      Goodman, M. B. Sensation is painless. *Trends Neurosci* **26**, 643-645 (2003).

490    2      Hall, D. H. & Treinin, M. How does morphology relate to function in sensory

491              arbors? *Trends Neurosci* **34**, 443-451, doi:S0166-2236(11)00108-1

492              [pii]10.1016/j.tins.2011.07.004 (2011).

493   3   Ruschel, J., Hellal, F., Flynn, K. C., Dupraz, S., Elliott, D. A., Tedeschi, A.,
494       Bates, M., Sliwinski, C., Brook, G., Dobrindt, K., Peitz, M., Brustle, O.,
495       Norenberg, M. D., Blesch, A., Weidner, N., Bunge, M. B., Bixby, J. L. &
496       Bradke, F. Axonal regeneration. Systemic administration of epothilone B
497       promotes axon regeneration after spinal cord injury. *Science* **348**, 347-352,
498       doi:10.1126/science.aaa2958 (2015).
499   4   Park, K. K., Liu, K., Hu, Y., Smith, P. D., Wang, C., Cai, B., Xu, B.,
500       Connolly, L., Kramvis, I., Sahin, M. & He, Z. Promoting axon regeneration in
501       the adult CNS by modulation of the PTEN/mTOR pathway. *Science* **322**, 963-
502       966 (2008).
503   5   Taylor, A. M., Blurton-Jones, M., Rhee, S. W., Cribbs, D. H., Cotman, C. W.
504       & Jeon, N. L. A microfluidic culture platform for CNS axonal injury,
505       regeneration and transport. *Nat Methods* **2**, 599-605, doi:nmeth777
506       [pii]10.1038/nmeth777 (2005).
507   6   Li, S., Yang, C., Zhang, L., Gao, X., Wang, X., Liu, W., Wang, Y., Jiang, S.,
508       Wong, Y. H., Zhang, Y. & Liu, K. Promoting axon regeneration in the adult
509       CNS by modulation of the melanopsin/GPCR signaling. *Proc Natl Acad Sci U*
510       *S A* **113**, 1937-1942, doi:10.1073/pnas.1523645113 (2016).
511   7   Coleman, M. P. & Freeman, M. R. Wallerian degeneration, wld(s), and nmnat.
512       *Annual review of neuroscience* **33**, 245-267, doi:10.1146/annurev-neuro-
513       060909-153248 (2010).
514   8   Wu, Z., Ghosh-Roy, A., Yanik, M. F., Zhang, J. Z., Jin, Y. & Chisholm, A. D.
515       Caenorhabditis elegans neuronal regeneration is influenced by life stage,
516       ephrin signaling, and synaptic branching. *Proc Natl Acad Sci U S A* **104**,
517       15132-15137 (2007).
518   9   Yan, D., Wu, Z., Chisholm, A. D. & Jin, Y. The DLK-1 kinase promotes
519       mRNA stability and local translation in C. elegans synapses and axon
520       regeneration. *Cell* **138**, 1005-1018, doi:S0092-8674(09)00723-5
521       [pii]10.1016/j.cell.2009.06.023 (2009).
522   10  Hammarlund, M. & Jin, Y. Axon regeneration in C. elegans. *Curr Opin*
523       *Neurobiol* **27**, 199-207, doi:10.1016/j.conb.2014.04.001 (2014).
524   11  Edwards, T. J. & Hammarlund, M. Syndecan promotes axon regeneration by
525       stabilizing growth cone migration. *Cell reports* **8**, 272-283,
526       doi:10.1016/j.celrep.2014.06.008 (2014).
527   12  Hammarlund, M., Nix, P., Hauth, L., Jorgensen, E. M. & Bastiani, M. Axon
528       regeneration requires a conserved MAP kinase pathway. *Science* **323**, 802-
529       806, doi:10.1126/science.1165527 (2009).
530   13  Bedi, S. S. & Glanzman, D. L. Axonal rejoining inhibits injury-induced long-
531       term changes in Aplysia sensory neurons in vitro. *J Neurosci* **21**, 9667-9677
532       (2001).
533   14  Hoy, R. R., Bittner, G. D. & Kennedy, D. Regeneration in crustacean
534       motoneurons: evidence for axonal fusion. *Science* **156**, 251-252 (1967).
535   15  Ghosh-Roy, A. & Chisholm, A. D. Caenorhabditis elegans: a new model
536       organism for studies of axon regeneration. *Dev Dyn* **239**, 1460-1464,
537       doi:10.1002/dvdy.22253 (2010).
538   16  Yanik, M. F., Cinar, H., Cinar, H. N., Chisholm, A. D., Jin, Y. & Ben-Yakar,
539       A. Neurosurgery: functional regeneration after laser axotomy. *Nature* **432**, 822
540       (2004).
541   17  Neumann, B., Coakley, S., Giordano-Santini, R., Linton, C., Lee, E. S.,
542       Nakagawa, A., Xue, D. & Hilliard, M. A. EFF-1-mediated regenerative axonal

21

543    fusion requires components of the apoptotic pathway. *Nature* **517**, 219-222
544    (2015).
545  18  Neumann, B., Nguyen, K. C., Hall, D. H., Ben-Yakar, A. & Hilliard, M. A.
546    Axonal regeneration proceeds through specific axonal fusion in transected C.
547    elegans neurons. *Dev Dyn* **240**, 1365-1372, doi:10.1002/dvdy.22606 (2011).
548  19  Bourgeois, F. & Ben-Yakar, A. Femtosecond laser nanoaxotomy properties
549    and their effect on axonal recovery in C. elegans. *Opt Express* **15**, 8521-8531
550    (2007).
551  20  Ghosh-Roy, A., Wu, Z., Goncharov, A., Jin, Y. & Chisholm, A. D. Calcium
552    and cyclic AMP promote axonal regeneration in Caenorhabditis elegans and
553    require DLK-1 kinase. *J Neurosci* **30**, 3175-3183, doi:30/9/3175
554    [pii]10.1523/JNEUROSCI.5464-09.2010 (2010).
555  21  Nix, P., Hammarlund, M., Hauth, L., Lachnit, M., Jorgensen, E. M. &
556    Bastiani, M. Axon regeneration genes identified by RNAi screening in C.
557    elegans. *J Neurosci* **34**, 629-645, doi:10.1523/JNEUROSCI.3859-13.2014
558    (2014).
559  22  Gabel, C. V., Antoine, F., Chuang, C. F., Samuel, A. D. & Chang, C. Distinct
560    cellular and molecular mechanisms mediate initial axon development and
561    adult-stage axon regeneration in C. elegans. *Development* **135**, 1129-1136
562    (2008).
563  23  Standler, N. A. & Bernstein, J. J. Degeneration and regeneration of
564    motoneuron dendrites after ventral root crush: computer reconstruction of
565    dendritic fields. *Experimental neurology* **75**, 600-615 (1982).
566  24  Song, Y., Ori-McKenney, K. M., Zheng, Y., Han, C., Jan, L. Y. & Jan, Y. N.
567    Regeneration of Drosophila sensory neuron axons and dendrites is regulated
568    by the Akt pathway involving Pten and microRNA bantam. *Genes Dev* **26**,
569    1612-1625, doi:10.1101/gad.193243.112 (2012).
570  25  Stone, M. C., Albertson, R. M., Chen, L. & Rolls, M. M. Dendrite injury
571    triggers DLK-independent regeneration. *Cell reports* **6**, 247-253,
572    doi:10.1016/j.celrep.2013.12.022 (2014).
573  26  Stone, M. C., Nguyen, M. M., Tao, J., Allender, D. L. & Rolls, M. M. Global
574    up-regulation of microtubule dynamics and polarity reversal during
575    regeneration of an axon from a dendrite. *Mol Biol Cell* **21**, 767-777,
576    doi:10.1091/mbc.E09-11-0967 (2010).
577  27  Hall, G. F. & Cohen, M. J. Dendritic amputation redistributes sprouting
578    evoked by axotomy in lamprey central neurons. *J Neurosci* **8**, 3598-3606
579    (1988).
580  28  White, J. G., Southgate, E., Thomson, J. N. & Brenner, S. The structure of the
581    nervous system of Caenorhabditis elegans. *Philos. Trans. R. Soc. Lond. B
582    Biol. Sci* **314**, 1-340 (1986).
583  29  Halevi, S., McKay, J., Palfreyman, M., Yassin, L., Eshel, M., Jorgensen, E. &
584    Treinin, M. The C. elegans ric-3 gene is required for maturation of nicotinic
585    acetylcholine receptors. *Embo J* **21**, 1012-1020 (2002).
586  30  Tsalik, E. L., Niacaris, T., Wenick, A. S., Pau, K., Avery, L. & Hobert, O.
587    LIM homeobox gene-dependent expression of biogenic amine receptors in
588    restricted regions of the C. elegans nervous system. *Dev Biol* **263**, 81-102
589    (2003).
590  31  Yassin, L., Gillo, B., Kahan, T., Halevi, S., Eshel, M. & Treinin, M.
591    Characterization of the deg-3/des-2 receptor: a nicotinic acetylcholine receptor

592      that mutates to cause neuronal degeneration. *Mol Cell Neurosci* **17**, 589-599
593      (2001).

594   32  Oren-Suissa, M., Hall, D., Treinin, M., Shemer, G. & Podbilewicz, B. The
595      Fusogen EFF-1 Controls Sculpting of Mechanosensory Dendrites. *Science*
596      **328**, 1285-1288, doi:10.1126/science.1189095 (2010).

597   33  Smith, C. J., Watson, J. D., Spencer, W. C., O'Brien, T., Cha, B., Albeg, A.,
598      Treinin, M. & Miller, D. M., 3rd. Time-lapse imaging and cell-specific
599      expression profiling reveal dynamic branching and molecular determinants of
600      a multi-dendritic nociceptor in C. elegans. *Dev Biol* **345**, 18-33, doi:S0012-
601      1606(10)00805-5 [pii]10.1016/j.ydbio.2010.05.502 (2010).

602   34  Albeg, A., Smith, C., Chatzigeorgiou, M., Feitelson, D. G., Hall, D. H.,
603      Schafer, W. R., Miller, D. M., 3rd & Treinin, M. C. elegans multi-dendritic
604      sensory neurons: Morphology and function. *Mol Cell Neurosci* **46**, 308-317,
605      doi:S1044-7431(10)00246-0 [pii]10.1016/j.mcn.2010.10.001 (2011).

606   35  Pujadas, L., Gruart, A., Bosch, C., Delgado, L., Teixeira, C. M., Rossi, D., de
607      Lecea, L., Martinez, A., Delgado-Garcia, J. M. & Soriano, E. Reelin regulates
608      postnatal neurogenesis and enhances spine hypertrophy and long-term
609      potentiation. *J Neurosci* **30**, 4636-4649, doi:30/13/4636
610      [pii]10.1523/JNEUROSCI.5284-09.2010 (2010).

611   36  Maniar, T. A., Kaplan, M., Wang, G. J., Shen, K., Wei, L., Shaw, J. E.,
612      Koushika, S. P. & Bargmann, C. I. UNC-33 (CRMP) and ankyrin organize
613      microtubules and localize kinesin to polarize axon-dendrite sorting. *Nat*
614      *Neurosci* **15**, 48-56, doi:10.1038/nn.2970 (2012).

615   37  Way, J. C. & Chalfie, M. The mec-3 gene of Caenorhabditis elegans requires
616      its own product for maintained expression and is expressed in three neuronal
617      cell types. *Genes Dev* **3**, 1823-1833 (1989).

618   38  Chatzigeorgiou, M., Yoo, S., Watson, J. D., Lee, W. H., Spencer, W. C.,
619      Kindt, K. S., Hwang, S. W., Miller, D. M., 3rd, Treinin, M., Driscoll, M. &
620      Schafer, W. R. Specific roles for DEG/ENaC and TRP channels in touch and
621      thermosensation in C. elegans nociceptors. *Nature neuroscience* **13**, 861-868,
622      doi:10.1038/nn.2581 (2010).

623   39  Chatzigeorgiou, M. & Schafer, W. R. Lateral facilitation between primary
624      mechanosensory neurons controls nose touch perception in C. elegans. *Neuron*
625      **70**, 299-309, doi:10.1016/j.neuron.2011.02.046 (2011).

626   40  Liang, X., Dong, X., Moerman, D. G., Shen, K. & Wang, X. Sarcomeres
627      Pattern Proprioceptive Sensory Dendritic Endings through UNC-52/Perlecan
628      in C. elegans. *Dev Cell* **33**, 388-400, doi:10.1016/j.devcel.2015.03.010 (2015).

629   41  Dong, X., Liu, O. W., Howell, A. S. & Shen, K. An extracellular adhesion
630      molecule complex patterns dendritic branching and morphogenesis. *Cell* **155**,
631      296-307, doi:10.1016/j.cell.2013.08.059 (2013).

632   42  Smith, C. J., Watson, J. D., VanHoven, M. K., Colon-Ramos, D. A. & Miller,
633      D. M., 3rd. Netrin (UNC-6) mediates dendritic self-avoidance. *Nat Neurosci*
634      **15**, 731-737, doi:10.1038/nn.3065 (2012).

635   43  Aguirre-Chen, C., Bulow, H. E. & Kaprielian, Z. C. elegans bicd-1, homolog
636      of the Drosophila dynein accessory factor Bicaudal D, regulates the branching
637      of PVD sensory neuron dendrites. *Development* **138**, 507-518,
638      doi:10.1242/dev.060939 (2011).

639   44  Salzberg, Y., Diaz-Balzac, C. A., Ramirez-Suarez, N. J., Attreed, M., Tecle,
640      E., Desbois, M., Kaprielian, Z. & Bulow, H. E. Skin-Derived Cues Control

23

641    Arborization of Sensory Dendrites in Caenorhabditis elegans. *Cell* **155**, 308-
642    320, doi:10.1016/j.cell.2013.08.058 (2013).
643  45  Taylor, C. A., Yan, J., Howell, A. S., Dong, X. & Shen, K. RAB-10 Regulates
644    Dendritic Branching by Balancing Dendritic Transport. *PLoS Genet* **11**,
645    e1005695, doi:10.1371/journal.pgen.1005695 (2015).
646  46  Dong, X., Chiu, H., Park, Y. J., Zou, W., Zou, Y., Ozkan, E., Chang, C. &
647    Shen, K. Precise regulation of the guidance receptor DMA-1 by KPC-1/Furin
648    instructs dendritic branching decisions. *eLife* **5**, doi:10.7554/eLife.11008
649    (2016).
650  47  Smurova, K. & Podbilewicz, B. RAB-5- and DYNAMIN-1-Mediated
651    Endocytosis of EFF-1 Fusogen Controls Cell-Cell Fusion. *Cell reports* **14**,
652    1517-1527, doi:10.1016/j.celrep.2016.01.027 (2016).
653  48  Podbilewicz, B. Virus and Cell Fusion Mechanisms. *Annual Review of Cell
654    and Developmental Biology* **30**, 111-139 (2014).
655  49  Shemer, G., Suissa, M., Kolotuev, I., Nguyen, K. C. Q., Hall, D. H. &
656    Podbilewicz, B. EFF-1 is sufficient to initiate and execute tissue-specific cell
657    fusion in *C. elegans*. *Curr Biol* **14**, 1587-1591 (2004).
658  50  Mohler, W. A., Shemer, G., del Campo, J., Valansi, C., Opoku-Serebuoh, E.,
659    Scranton, V., Assaf, N., White, J. G. & Podbilewicz, B. The type I membrane
660    protein EFF-1 is essential for developmental cell fusion in *C. elegans*. *Dev
661    Cell* **2**, 355-362 (2002).
662  51  Shinn-Thomas, J. H., Del Campo, J. J., Wang, J. & Mohler, W. A. The EFF-
663    1A Cytoplasmic Domain Influences Hypodermal Cell Fusions in C. elegans
664    But Is Not Dependent on 14-3-3 Proteins. *PLoS One* **11**, e0146874,
665    doi:10.1371/journal.pone.0146874 (2016).
666  52  Shinn-Thomas, J. H. & Mohler, W. A. New insights into the mechanisms and
667    roles of cell-cell fusion. *Int Rev Cell Mol Biol* **289**, 149-209,
668    doi:10.1016/B978-0-12-386039-2.00005-5 (2011).
669  53  Rasmussen, J. P., English, K., Tenlen, J. R. & Priess, J. R. Notch signaling and
670    morphogenesis of single-cell tubes in the C. elegans digestive tract. *Dev Cell*
671    **14**, 559-569 (2008).
672  54  Sapir, A., Choi, J., Leikina, E., Avinoam, O., Valansi, C., Chernomordik, L.
673    V., Newman, A. P. & Podbilewicz, B. AFF-1, a FOS-1-Regulated Fusogen,
674    Mediates Fusion of the Anchor Cell in C. elegans. *Dev Cell* **12**, 683-698
675    (2007).
676  55  Stone, C. E., Hall, D. H. & Sundaram, M. V. Lipocalin signaling controls
677    unicellular tube development in the Caenorhabditis elegans excretory system.
678    *Dev Biol* **329**, 201-211, doi:10.1016/j.ydbio.2009.02.030 (2009).
679  56  Bradbury, E. J., Moon, L. D., Popat, R. J., King, V. R., Bennett, G. S., Patel,
680    P. N., Fawcett, J. W. & McMahon, S. B. Chondroitinase ABC promotes
681    functional recovery after spinal cord injury. *Nature* **416**, 636-640 (2002).
682  57  Cajal, S. R. *Histología del sistema nervioso del hombre y de los vertebrados*.
683    2007 edn, Vol. 1 (Ministerio de Sanidad y Consumo, 1899).
684  58  Fernandez-Gonzalez, A., La Spada, A. R., Treadaway, J., Higdon, J. C.,
685    Harris, B. S., Sidman, R. L., Morgan, J. I. & Zuo, J. Purkinje cell degeneration
686    (pcd) phenotypes caused by mutations in the axotomy-induced gene, Nna1.
687    *Science* **295**, 1904-1906 (2002).
688  59  Devor, M. Neuroplasticity in the rearrangement of olfactory tract fibers after
689    neonatal transection in hamsters. *The Journal of comparative neurology* **166**,
690    49-72 (1976).

| 691 | 60 | Oren-Suissa, M. & Podbilewicz, B. Evolution of programmed cell fusion: Common mechanisms and distinct functions. *Developmental Dynamics* **239**, 1515-1528, doi:10.1002/dvdy.22284 (2010). |

693

694 61 Nawabi, H., Zukor, K. & He, Z. No simpler than mammals: axon and dendrite regeneration in Drosophila. *Genes Dev* **26**, 1509-1514, doi:10.1101/gad.198150.112 (2012).

697 62 Hilliard, M. A. Axonal degeneration and regeneration: a mechanistic tug-of-war. *J Neurochem* **108**, 23-32, doi:10.1111/j.1471-4159.2008.05754.x (2009).

699 63 Podbilewicz, B., Leikina, E., Sapir, A., Valansi, C., Suissa, M., Shemer, G. & Chernomordik, L. V. The C. elegans developmental fusogen EFF-1 mediates homotypic fusion in heterologous cells and in vivo. *Dev Cell* **11**, 471-481 (2006).

703 64 Avinoam, O., Fridman, K., Valansi, C., Abutbul, I., Zeev-Ben-Mordehai, T., Maurer, U. E., Sapir, A., Danino, D., Gruenewald, K., White, J. M. & Podbilewicz, B. Conserved Eukaryotic Fusogens Can Fuse Viral Envelopes to Cells. *Science* **332**, 589-592, doi:10.1126/science.1202333 (2011).

707 65 Clavel, F. & Charneau, P. Fusion from without directed by human immunodeficiency virus particles. *J Virol* **68**, 1179-1185 (1994).

709 66 Bratt, M. A. & Gallaher, W. R. Preliminary analysis of the requirements for fusion from within and fusion from without by Newcastle disease virus. *Proc Natl Acad Sci U S A* **64**, 536-543 (1969).

712 67 White, J., Matlin, K. & Helenius, A. Cell fusion by Semliki Forest, influenza, and vesicular stomatitis viruses. *J Cell Biol* **89**, 674-679 (1981).

714 68 Tkach, M. & Thery, C. Communication by Extracellular Vesicles: Where We Are and Where We Need to Go. *Cell* **164**, 1226-1232, doi:10.1016/j.cell.2016.01.043 (2016).

717 69 Miyado, K., Yoshida, K., Yamagata, K., Sakakibara, K., Okabe, M., Wang, X., Miyamoto, K., Akutsu, H., Kondo, T., Takahashi, Y., Ban, T., Ito, C., Toshimori, K., Nakamura, A., Ito, M., Miyado, M., Mekada, E. & Umezawa, A. The fusing ability of sperm is bestowed by CD9-containing vesicles released from eggs in mice. *Proc Natl Acad Sci U S A* **105**, 12921-12926 (2008).

723 70 Kwon, S. H., Liu, K. D. & Mostov, K. E. Intercellular Transfer of GPRC5B via Exosomes Drives HGF-Mediated Outward Growth. *Curr Biol* **24**, 199-204, doi:10.1016/j.cub.2013.12.010 (2014).

726 71 Liegeois, S., Benedetto, A., Garnier, J. M., Schwab, Y. & Labouesse, M. The V0-ATPase mediates apical secretion of exosomes containing Hedgehog-related proteins in Caenorhabditis elegans. *J Cell Biol* **173**, 949-961, doi:10.1083/jcb.200511072 (2006).

730 72 Beveridge, T. J. Structures of gram-negative cell walls and their derived membrane vesicles. *J Bacteriol* **181**, 4725-4733 (1999).

732 73 Hyenne, V., Apaydin, A., Rodriguez, D., Spiegelhalter, C., Hoff-Yoessle, S., Diem, M., Tak, S., Lefebvre, O., Schwab, Y., Goetz, J. G. & Labouesse, M. RAL-1 controls multivesicular body biogenesis and exosome secretion. *J Cell Biol* **211**, 27-37, doi:10.1083/jcb.201504136 (2015).

736 74 Wang, J., Silva, M., Haas, L. A., Morsci, N. S., Nguyen, K. C., Hall, D. H. & Barr, M. M. C. elegans ciliated sensory neurons release extracellular vesicles that function in animal communication. *Curr Biol* **24**, 519-525, doi:10.1016/j.cub.2014.01.002 (2014).

740  75  Kosinski, M., McDonald, K., Schwartz, J., Yamamoto, I. & Greenstein, D. C.
741      elegans sperm bud vesicles to deliver a meiotic maturation signal to distant
742      oocytes. *Development* **132**, 3357-3369, doi:10.1242/dev.01916 (2005).
743  76  Mapes, J., Chen, Y. Z., Kim, A., Mitani, S., Kang, B. H. & Xue, D. CED-1,
744      CED-7, and TTR-52 regulate surface phosphatidylserine expression on
745      apoptotic and phagocytic cells. *Curr Biol* **22**, 1267-1275,
746      doi:10.1016/j.cub.2012.05.052 (2012).
747  77  Wehman, A. M., Poggioli, C., Schweinsberg, P., Grant, B. D. & Nance, J. The
748      P4-ATPase TAT-5 inhibits the budding of extracellular vesicles in C. elegans
749      embryos. *Curr Biol* **21**, 1951-1959, doi:10.1016/j.cub.2011.10.040 (2011).
750  78  Fridman, K. *Ultrastructure and function of AFF-1 and EFF-1 in membrane*
751      *remodeling* MSc thesis, Technion - Israel Institute of Technology, (2012).
752  79  Avinoam, O. & Podbilewicz, B. Eukaryotic cell-cell fusion families. *Curr Top*
753      *Membr* **68**, 209-234, doi:B978-0-12-385891-7.00009-X [pii]10.1016/B978-0-
754      12-385891-7.00009-X (2011).
755  80  Jorgensen, E. M. & Rankin, C. in *C. elegans II*  (eds D. L. Riddle, T.
756      Blumenthal, B. J. Meyer, & J. R. Priess)  (1997).
757  81  Hayashi, Y., Hirotsu, T., Iwata, R., Kage-Nakadai, E., Kunitomo, H., Ishihara,
758      T., Iino, Y. & Kubo, T. A trophic role for Wnt-Ror kinase signaling during
759      developmental pruning in Caenorhabditis elegans. *Nat Neurosci* **12**, 981-987,
760      doi:10.1038/nn.2347 (2009).
761  82  Tessier, C. R. & Broadie, K. Drosophila fragile X mental retardation protein
762      developmentally regulates activity-dependent axon pruning. *Development* **135**,
763      1547-1557 (2008).
764  83  Singh, K. K., Park, K. J., Hong, E. J., Kramer, B. M., Greenberg, M. E.,
765      Kaplan, D. R. & Miller, F. D. Developmental axon pruning mediated by
766      BDNF-p75NTR-dependent axon degeneration. *Nat Neurosci* **11**, 649-658
767      (2008).
768  84  Schuldiner, O., Berdnik, D., Levy, J. M., Wu, J. S., Luginbuhl, D., Gontang,
769      A. C. & Luo, L. piggyBac-based mosaic screen identifies a postmitotic
770      function for cohesin in regulating developmental axon pruning. *Dev Cell* **14**,
771      227-238 (2008).
772  85  Helton, T. D., Otsuka, T., Lee, M. C., Mu, Y. & Ehlers, M. D. Pruning and
773      loss of excitatory synapses by the parkin ubiquitin ligase. *Proc Natl Acad Sci*
774      *U S A* **105**, 19492-19497 (2008).
775  86  Zhai, Q., Wang, J., Kim, A., Liu, Q., Watts, R., Hoopfer, E., Mitchison, T.,
776      Luo, L. & He, Z. Involvement of the ubiquitin-proteasome system in the early
777      stages of wallerian degeneration. *Neuron* **39**, 217-225 (2003).
778  87  Martin, S. M., O'Brien, G. S., Portera-Cailliau, C. & Sagasti, A. Wallerian
779      degeneration of zebrafish trigeminal axons in the skin is required for
780      regeneration and developmental pruning. *Development* **137**, 3985-3994,
781      doi:10.1242/dev.053611 (2010).
782  88  Kage, E., Hayashi, Y., Takeuchi, H., Hirotsu, T., Kunitomo, H., Inoue, T.,
783      Arai, H., Iino, Y. & Kubo, T. MBR-1, a novel helix-turn-helix transcription
784      factor, is required for pruning excessive neurites in Caenorhabditis elegans.
785      *Curr Biol* **15**, 1554-1559, doi:10.1016/j.cub.2005.07.057 (2005).
786  89  Paltsyn, A., Komissarova, S., Dubrovin, I. & Kubatiev, A. Increased cell
787      fusion in cerebral cortex may contribute to poststroke regeneration. *Stroke*
788      *research and treatment* **2013**, 869327, doi:10.1155/2013/869327 (2013).

789   90   Yaniv, S. P., Issman-Zecharya, N., Oren-Suissa, M., Podbilewicz, B. &
790        Schuldiner, O. Axon Regrowth during Development and Regeneration
791        Following Injury Share Molecular Mechanisms. *Curr Biol* **22**, 1774-1782,
792        doi:10.1016/j.cub.2012.07.044 (2012).
793   91   Bradke, F., Fawcett, J. W. & Spira, M. E. Assembly of a new growth cone
794        after axotomy: the precursor to axon regeneration. *Nat Rev Neurosci* **13**, 183-
795        193, doi:10.1038/nrn3176 (2012).
796   92   Mar, F. M., Bonni, A. & Sousa, M. M. Cell intrinsic control of axon
797        regeneration. *EMBO reports* **15**, 254-263, doi:10.1002/embr.201337723
798        (2014).
799   93   Wang, H. & Macagno, E. R. A detached branch stops being recognized as self
800        by other branches of a neuron. *Journal of neurobiology* **35**, 53-64 (1998).
801   94   Moritz, C. T., Perlmutter, S. I. & Fetz, E. E. Direct control of paralysed
802        muscles by cortical neurons. *Nature* **456**, 639-642 (2008).
803   95   Brenner, S. The genetics of *Caenorhabditis elegans*. *Genetics* **77**, 71-94
804        (1974).
805   96   Sulston, J. & Hodgkin, J. in *The Nematode Caenorhabditis elegans*  (ed W.B.
806        Wood)  587-606 (Cold Spring Harbor Laboratory, 1988).
807   97   Yip, Z. C. & Heiman, M. G. Duplication of a Single Neuron in C. elegans
808        Reveals a Pathway for Dendrite Tiling by Mutual Repulsion. *Cell reports*,
809        doi:10.1016/j.celrep.2016.05.003 (2016).
810   98   Mello, C. & Fire, A. in *Methods in Cell Biology. Caenorhabditis elegans:*
811        *Model Biological Analysis of an Organism* Vol. 48  (eds H F Epstein & D C
812        Shakes)  451-482 (Academic Press, 1995).
813   99   Bond, S. R. & Naus, C. C. RF-Cloning.org: an online tool for the design of
814        restriction-free cloning projects. *Nucleic Acids Res* **40**, W209-213,
815        doi:10.1093/nar/gks396 (2012).
816   100  Petersen, L. K. & Stowers, R. S. A Gateway MultiSite recombination cloning
817        toolkit. *PLoS One* **6**, e24531, doi:10.1371/journal.pone.0024531 (2011).
818   101  McCarter, J., Bartlett, B., Dang, T. & Schedl, T. On the control of oocyte
819        meiotic maturation and ovulation in Caenorhabditis elegans. *Dev Biol* **205**,
820        111-128 (1999).
821   102  McCarter, J., Bartlett, B., Dang, T. & Schedl, T. Soma-germ cell interactions
822        in Caenorhabditis elegans: multiple events of hermaphrodite germline
823        development require the somatic sheath and spermathecal lineages. *Dev Biol*
824        **181**, 121-143 (1997).
825   103  Kirby, C., Kusch, M. & Kemphues, K. Mutations in the *par* genes of
826        *Caenorhabditis elegans* affect cytoplasmic reorganization during the first cell
827        cycle. *Dev. Biol.* **142**, 203-215 (1990).
828

829 **Figures**



Oren-Suissa Figure 1
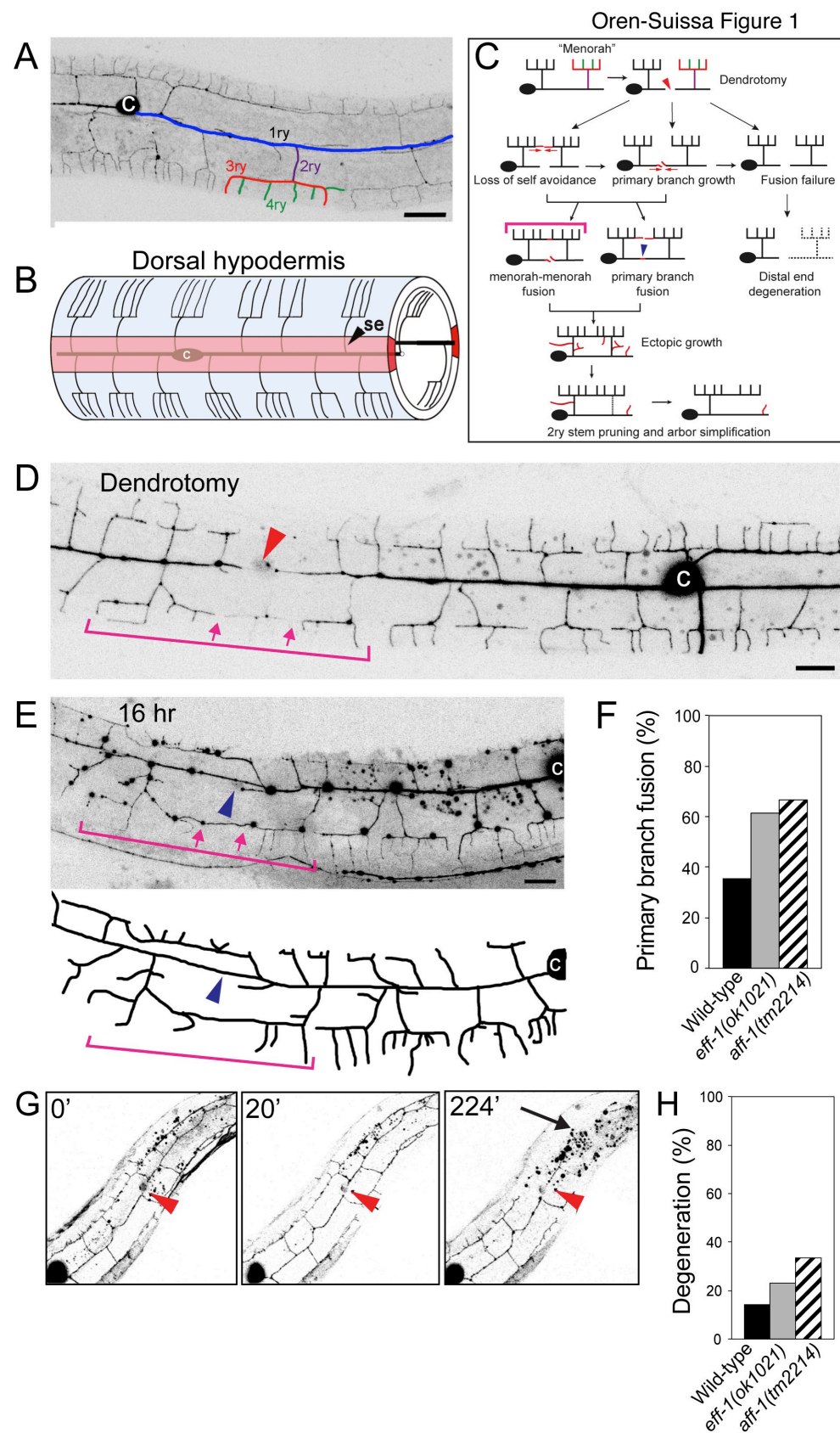
830
831

**Figure 1.**

**Dendrite regeneration of multibranched PVD neurons following laser microsurgery in *C. elegans***

**(A)** A wild-type animal expressing *DES-2::GFP*, illustrating the PVD neuron elaborate branching pattern (inverted image). Branches of one menorah are numbered primary to quaternary (1ry to 4ry), and color-coded: blue, purple, red, and green, respectively [32], c= cell body.

**(B)** Schematic model of hypodermal cells and PVD menorahs in a young adult, left view. The wild-type PVDs grow between the hypodermis (outer cylinder, light blue) and the basement membrane of the hypodermis (not shown), extending processes that branch out to form the menorah structures. In light red is the left hypodermal seam syncytium. Modified from [32], se= seam cells, c= cell body.

**(C)** Cartoon summarizing the different stages in PVD regeneration following injury. Two-photon dendrotomy (see Materials and methods) of the primary process (red arrowhead) leads to dynamic changes in the PVD arbor: loss of branch self-avoidance and growth is followed by primary branch fusion (blue arrowhead), menorah-menorah fusion (pink bracket), or both. There is an additional phase of dynamic growth and pruning, leading to arbor refinement. When the branches fail to fuse, the distal end undergoes degeneration.

**(D-E)** Primary and menorah-menorah fusion following dendrotomy. L4 animal just after surgery (**D**) and 16 hr post-surgery (**E**). Red arrowhead marks the site of dendrotomy. Blue arrowhead marks reconnection site of dendrotomy.

**(E)** The severed distal and proximal ends of the primary branch reconnected (blue arrowhead). Distal and proximal menorahs fused to form an additional connection between the soma and distal end (Pink arrows and bracket).

**(F)** Percentage of primary branch fusion during regeneration in wild type (n=14), *eff-1(ok1021)* (n=13) and *aff-1(tm2214)* (n=12) dendrotomized animals.

**(G)** Live imaging of an injured young-adult animal in which reconnection was unsuccessful, and degeneration of the distal arbor occurred. Time after injury is indicated in minutes. Red arrowhead– site of injury. Arrow– degenerating arbor. Images are taken from **Movie 3**. Posterior is up and dorsal is left. Scale bars represent 20 μm in (A) and 10 μm in (D-E).

**(H)** Percentage of animals with degenerating distal end following dendrotomy in wild type, *eff-1(ok1021)* and *aff-1(tm2214)* animals.

29

877
878

879   **Figure 2.**

880
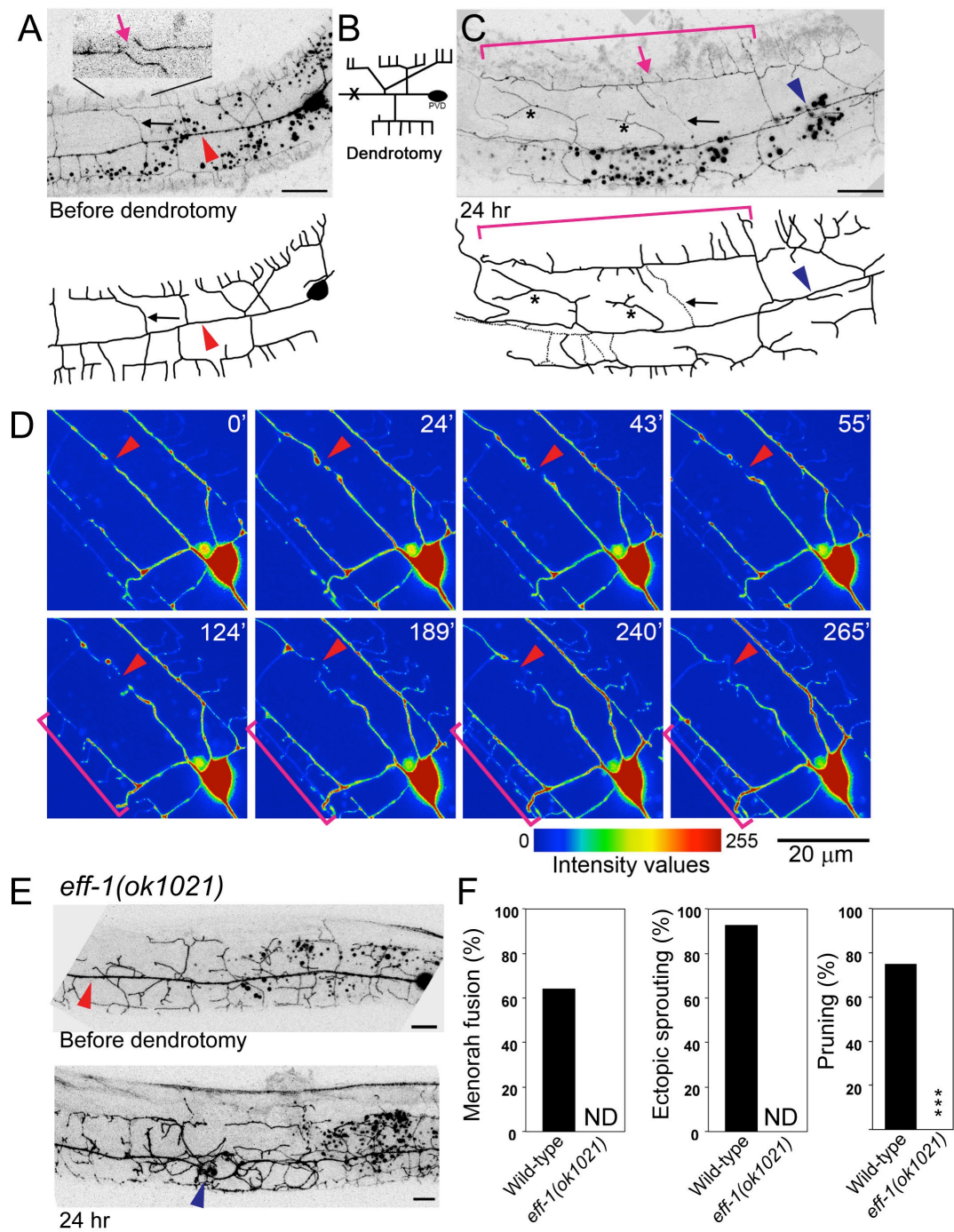
881   **The dynamic pathway of PVD regeneration after injury**

882

883   **(A-C)** Dendrotomy of an L4 animal resulted in menorah-menorah fusion.

884

885   **(A)** Just prior to the injury separate menorahs can be seen (pink arrow in inset). Red
886   arrowhead points to the lesion site.

887

888   **(B)** Schematic showing the site of injury (marked with an X).
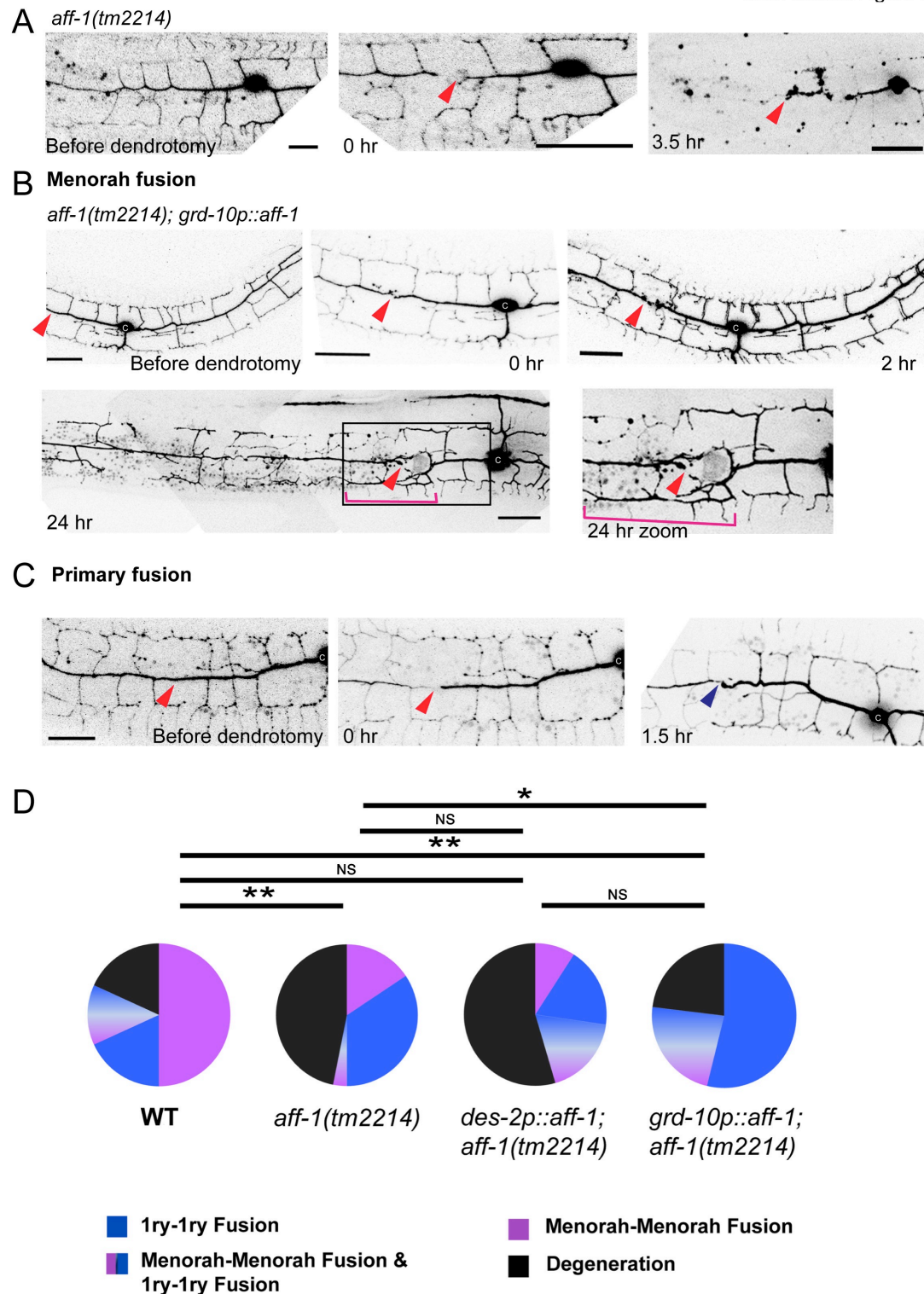
889

890   **(C)** Formation of giant menorahs (pink bracket) and ectopic sprouting (asterisks)
891   within 24 hr. Pink arrow points to the site of loss of self-avoidance. Blue arrowhead
892   points to the site of 1ry-1ry fusion. Pruning of secondary branches also occurs (black
893   arrow, dotted lines, also marked in (**A**)).

894

895   **(D)** Intensity values view of images from a time-lapse movie of injured L4 wild-type
896   worm (**Movie 4**). Time after injury is shown at the upper right corner in minutes.
897   Arrowheads point to injury site and pruning of branches. Brackets mark two
898   menorahs from distal and proximal ends bypassing the break and contacting one
899   another.

900

901   **(E)** *eff-1* animal before and 24 hr after dendrotomy. There is a successful reconnection
902   of the severed primary branch (arrowhead) and pruning failure (the arbor does not
903   undergo simplification). Scale bars represent 10 μm.

904

905   **(F)** Dendrotomy-induced phenotypes in *eff-1(ok1021)* animals. Menorah-menorah
906   fusion, percentage of animals that contained fused giant menorahs; ectopic sprouting,
907   fraction of animals showing growth of additional processes; pruning, percentage of
908   animals in which PVD underwent branch refinement after fusion. In *eff-1(ok1021)*
909   mutants there is excess branching and disorganized branch structure [32], thus we could
910   not determine (ND) whether menorah-menorah connections and ectopic sprouting
911   occurred. ***$P<0.001$, Fisher's exact test. n values: 14, 13 animals for wild-type and
912   *eff-1(ok1021),* respectively.

913

31

**A** *aff-1(tm2214)*

Before dendrotomy | 0 hr | 3.5 hr

**B** Menorah fusion

*aff-1(tm2214); grd-10p::aff-1*

Before dendrotomy | 0 hr | 2 hr

24 hr | 24 hr zoom

**C** Primary fusion

Before dendrotomy | 0 hr | 1.5 hr

**D**

WT | *aff-1(tm2214)* | *des-2p::aff-1; aff-1(tm2214)* | *grd-10p::aff-1; aff-1(tm2214)*

■ 1ry-1ry Fusion
▮ Menorah-Menorah Fusion & 1ry-1ry Fusion
■ Menorah-Menorah Fusion
■ Degeneration

914
915

32

916 **Figure 3.**

917 *aff-1* **dendritic reconnection patterns are rescued cell non-autonomously**

918 **(A)** Dendrite regeneration following PVD nanosurgery in *aff-1(tm2214)* mutant
919 animal. PVD is shown before and after nanosurgery (t=0 and 3.5 hr). In non-injured
920 *aff-1* mutant animals PVD branching pattern is unaffected. After injury, fusion does
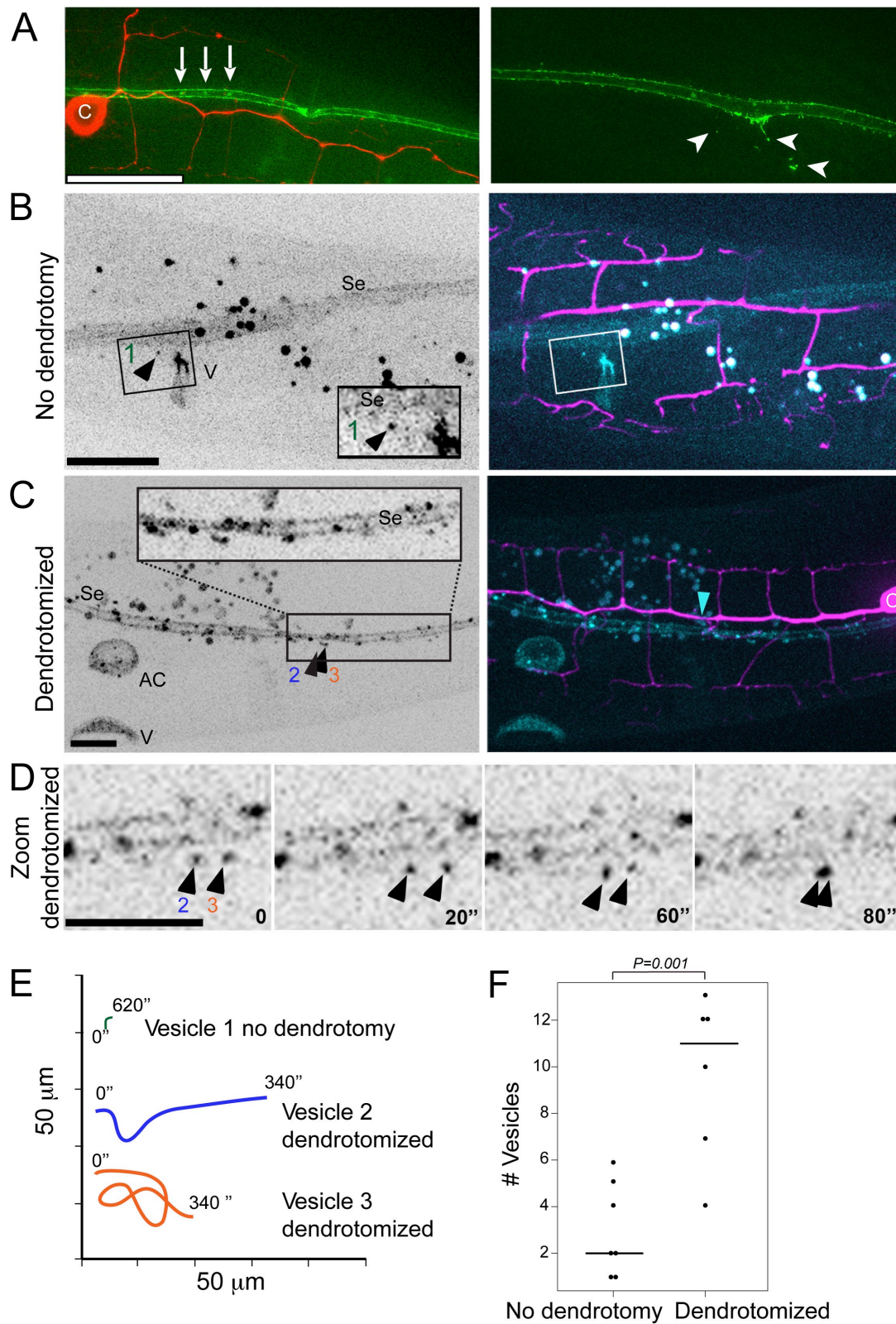921 not occur and the distal processes undergo degeneration (t=3.5 hr).
922

923 **(B)** Dendrite regeneration following PVD nanosurgery in *aff-1(tm2214); grd-10p::aff-*
924 *1* animals. PVD is shown before and after nanosurgery (t=0, 2, and 24 hr). PVD
925 reconnection occurred through fused menorahs (pink bracket). Red arrowhead marks
926 site of injury. Primary branches did not fuse (red arrowhead).
927

928 **(C)** Dendrite regeneration following PVD nanosurgery in *aff-1(tm2214); grd-*
929 *10p::aff-1* animals. PVD is shown before and after nanosurgery (t=0 and 1.5 hr). PVD
930 reconnection occurred through primary fusion (blue arrowhead).
931

932 **(D)** PVD post-injury outcomes displayed in color coded pie graphs as Magenta–
933 Menorah-Menorah fusion, Blue– primary-primary fusion, Magenta and Blue–
934 Menorah-Menorah fusion and primary-primary fusion, Black– degeneration. Wild
935 type n=22, *aff-1(tm2214)* n=32, *aff-1(tm2214);des-2p::aff*-n=11*, aff-1(tm2214); grd-*
936 *10p::aff-1* n=13. \*\* $P<0.01$; \* $P<0.05$; NS $P>0.05$. Dendrotomy site – red arrowhead,
937 fused menorah – pink bracket, primary fusion – blue arrowhead. Scale bars represent
938 20 μm. Statistics was calculated using the Freeman-Halton extension of the Fisher
939 exact probability test for a two-rows by four-columns contingency table,
940 http://vassarstats.net/fisher2x4.html.
941

33

942
943

34

**Figure 4.**

**AFF-1 protein dynamics during PVD regeneration**

**(A)** Superresolution structured illumination microscopy (SIM) image of aligned *AFF-1::GFP* (green) vesicles in the seam cells (left, white arrows) and *AFF-1::GFP* extracellular vesicles derived from the seam cells (right, white arrowheads ) in intact wild type animals. c, cell body. PVD is labeled in red.

**(B)** Spinning disk confocal images of *AFF-1::GFP* expression inside and outside the seam cells (Se), and in the vulva (V) of an intact L4 animal (left). *AFF-1::GFP* (cyan) expression in the seam cells and in vesicles near the seam cells is shown in a two channels merged image (right; PVD in magenta; **Movie 5**). Inset shows magnification of a single *AFF-1::GFP* vesicle near the seam cells (left, black arrowhead, numbered 1; **Movie 6**).

**(C)** *AFF-1::GFP* expression inside and outside the seam cells (Se), in the anchor cell (AC) and in the vulva (V) of a reconnected PVD L4 animal (left) is shown 2 hr post-dendrotomy in a spinning disk confocal image. *AFF-1::GFP* is expressed in vesicles inside and outside of the seam cells, in the anchor cell (AC) and in VulA ring (see **Movie 7**). Inset shows magnification of area with multiple vesicles, two are labeled (2,3) and shown in panels **(D-E).**

**(D)** Two *AFF-1::GFP* vesicles, numbered 2 and 3, are moving near the seam cells in a PVD-dendrotomized animal. Four time points are shown (0, 20, 60 and 80 sec; **Movie 8**).

**(E)** Vesicles dynamics (1, 2 and 3) is demonstrated in a color-coded graph during 340 seconds for vesicles 2 and 3 and 620 seconds for vesicle number 1. The plot illustrates vast differences between *AFF-1::GFP* vesicles movements in animals with an intact PVD versus *AFF-1::GFP* vesicles in PVD dendrotomized animals (**Movies 6 and 8)**.

**(F)** Dot Plot of the number of *AFF-1::GFP* vesicles outside *aff-1* expressing organs in animals with intact PVD versus in animals with dendrotomized PVD. The graph demonstrates statistical significant difference between the mean number of *aff-1::GFP* vesicles outside *aff-1* expressing organs such as seam cells, vulva, anchor cell and the uterus. $P=0.001$, statistics was calculated using the nonparametric Mann-Whitney test.
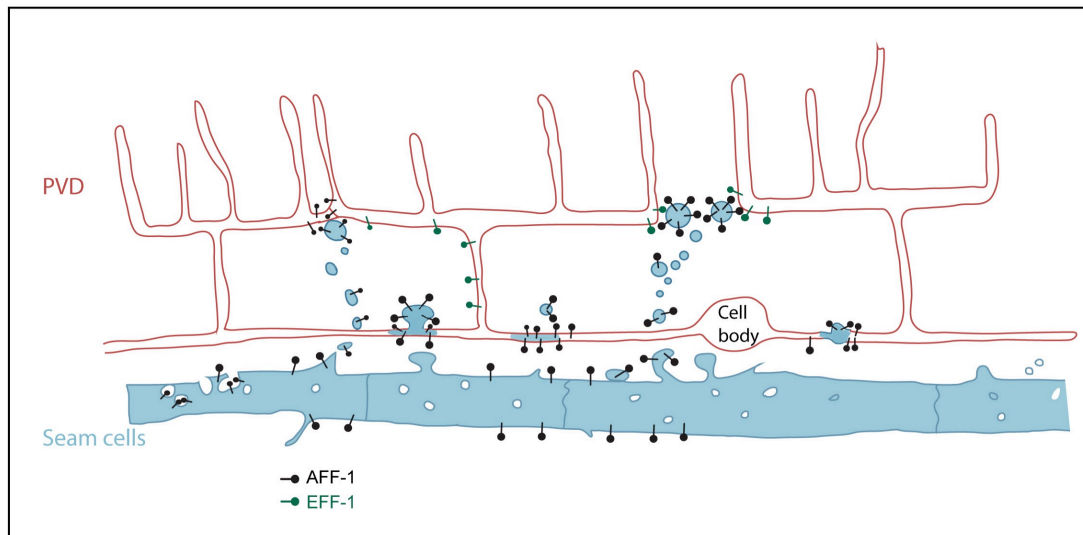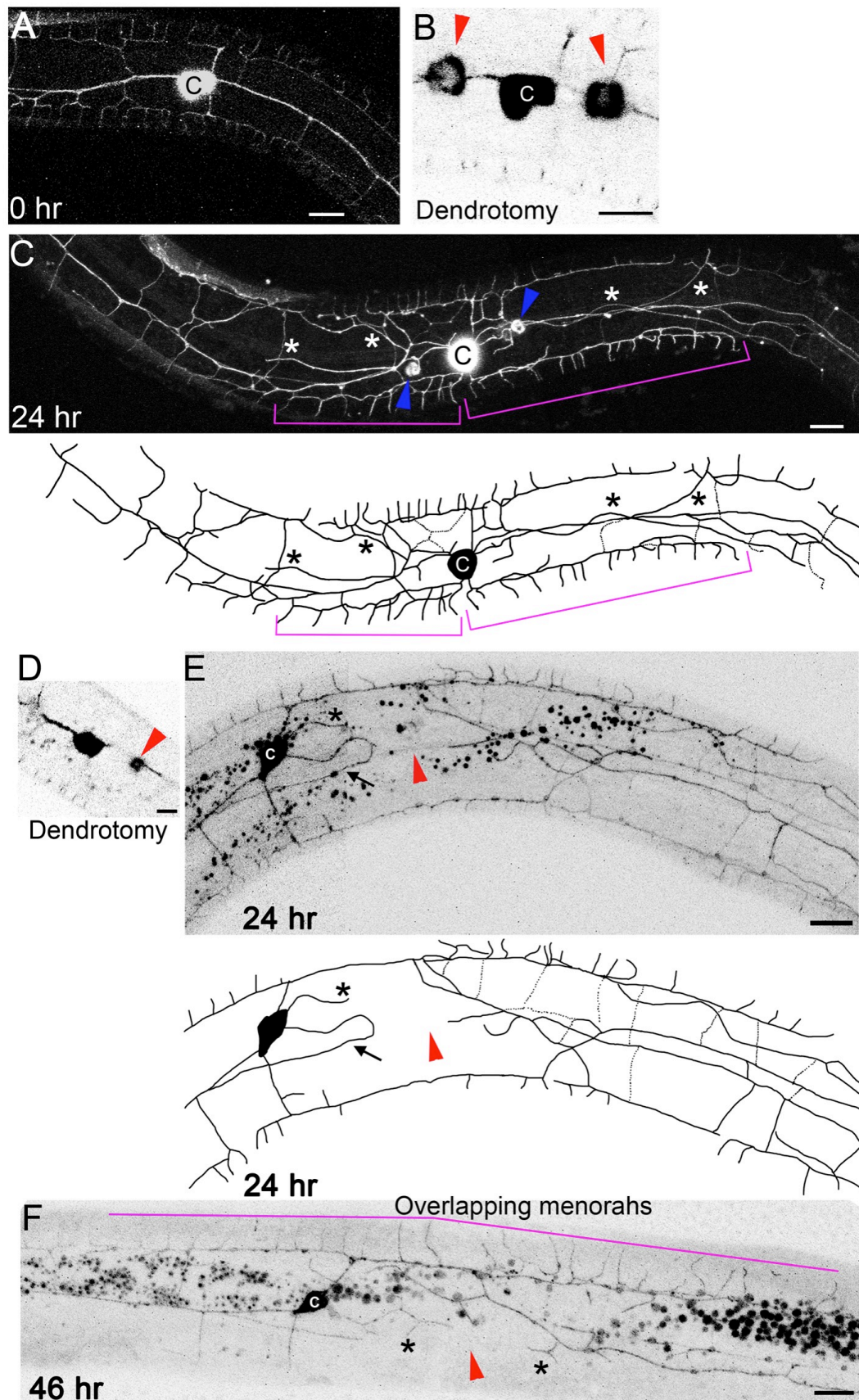
**Figure 5.**

**Model of AFF-1-mediated repair via extracellular vesicle-cell fusion**

PVD (red) is in close proximity to the epithelial seam cells (blue). AFF-1 (black pins) is expressed in seam cells and additional tissues, but not in the PVD. Upon injury, AFF-1-containing extracellular vesicles (EVs) are highly released from the seam cells. Some of these EVs reach the PVD and promote fusion of severed dendrites. EFF-1 (green pins) is expressed in the PVD but it does not act to fuse severed dendrites on its own. Instead it may collaborate with AFF-1-EVs. We propose that menorah-menorah fusion is mediated by AFF-1-EVs that merge with the structurally compatible EFF-1 expressed in the PVD. EFF-1-coated pseudotyped viruses can fuse with cells expressing AFF-1 on their surface and vice versa [64].

998    **Supplementary Figures**
999



1000
1001

1002    **Figure 1-figure supplement 1.**
1003
1004    **Dendritic amputation induces hyper-branching, loss of self-avoidance and giant**
1005    **overlapping menorahs**
1006
1007    **(A)** Wild-type animal before dendrotomy.
1008
1009    **(B)** Two laser-induced injuries of primary branches (red arrowheads, injury sites).
1010
1011    **(C)** Confocal projection and a schematic tracing of the same animal 24 hr post-
1012    surgery. Asterisks mark new sprouting from proximal and distal branches. Pink
1013    brackets, giant menorahs. Blue arrowheads, primary branch fusion.
1014
1015    **(D)** A different wild-type animal injured (red arrowhead) at the early L4 stage,
1016    recovered and analyzed 24 **(E)** and 46 hr **(F)** post-surgery. Black arrow, retrograde
1017    branch. The degenerating branches are represented as dotted lines in the schematic
1018    tracing. Scale bars represent 5 μm **(D)** and 10 μm **(A-C, E-F).**
1019
1020
1021
1022
1023
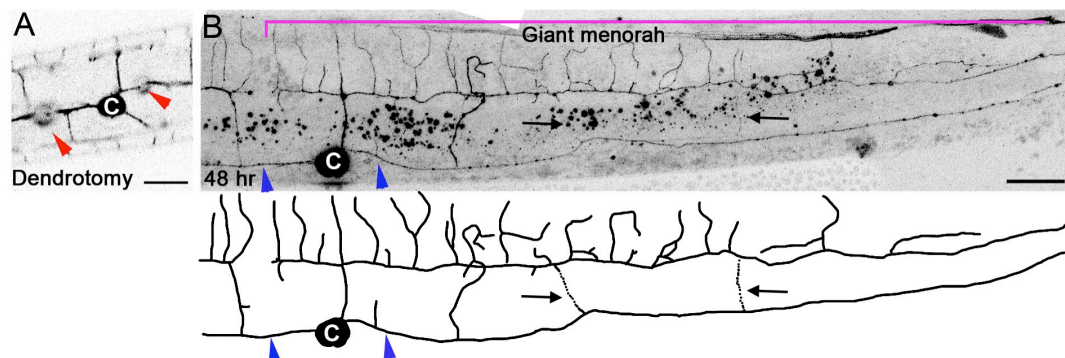


1024
1025
1026    **Figure 2- figure supplement 1.**
1027
1028    **Menorah fusion and 2ry stem pruning are part of the regeneration process of the**
1029    **PVDs following dendrotomy**
1030
1031    **(A)** Dendrotomy of an L4 wild-type animal. Red arrowheads point to sites of laser
1032    surgery.
1033
1034    **(B)** Analysis 48 hr post-surgery. Giant menorah can be seen (pink bracket); arrows
1035    (and dotted lines in the schematic tracing) point to secondary branches undergoing
1036    trimming. Blue arrowheads mark primary branch fusion at the sites of dendrotomy.
1037    Scale bars represent 10 μm.
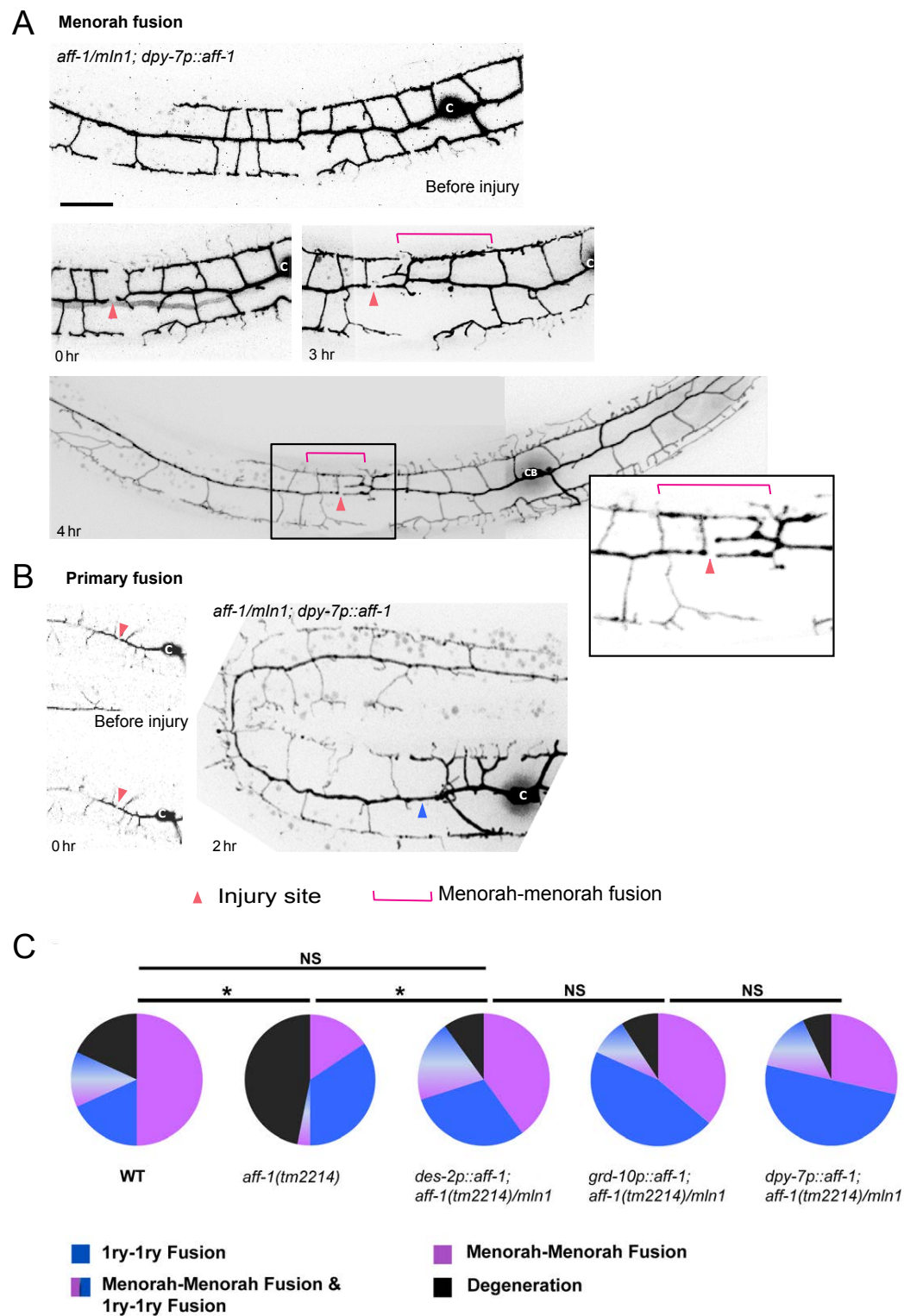1038
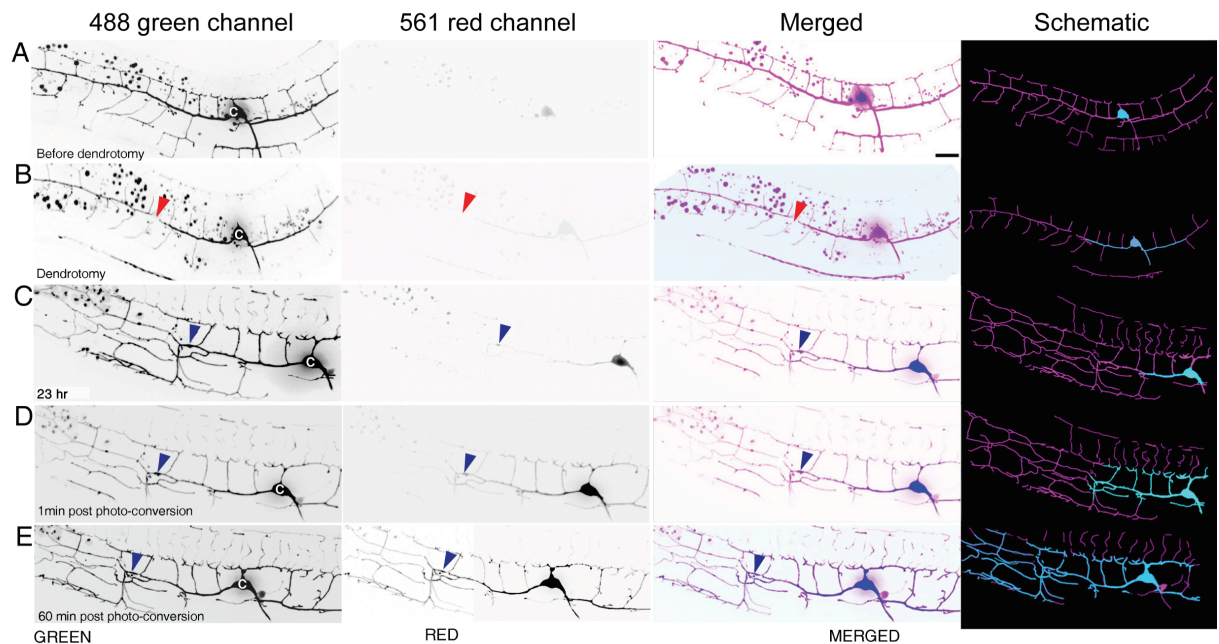
**Figure 2-figure supplement 2.**

**PVD dendrite reconnection confirmed by Kaede photoconversion**

A PVD primary dendrite of *ser-2prom3::Kaede* expressing animals was dendrotomized, the animal was recovered for 23 hr and the dendrite reconnection to its stump was assessed by Kaede photoconversion. The green Kaede form in the PVD cell body was irreversibly photo-converted to the red Kaede form using a 405nm laser with the Mosaic system and its spreading throughout the dendritic branches was followed 1 and 60 min post-photoconversion. Panels left to right are confocal reconstructions of a wild-type dendrotomized animal in the 488 green channel, 561 red channel, two channels merged view and a schematic representation of the merged view.

**(A)** Confocal reconstructions of the animal before dendrotomy, **(B)** immediately post dendrotomy, **(C)** 23 hr post-dendrotomy, **(D)** 1 min post Kaede photoconversion and **(E)** 60 min post Kaede photoconversion. Red Kaede form (cyan in merged and shematic representations), though diluted when spreading through the dendritic tree, can be observed beyond the reconnected site of injury in the distal part of the primary and higher ordered dendritic branches. Thus, Kaede photoconversion and diffusion beyond the injury site demonstrate fusion between the severed primary dendrite. In animals where reconnection failed photoconverted Kaede did not spread beyond the injury site (data not shown).
c, PVD cell body; red arrowhead, site of injury; blue arrowhead, site of primary branch fusion. In the merged and schematic columns: pink, green Kaede; cyan, photoconverted red Kaede.

A  **Menorah fusion**

*aff-1/mln1; dpy-7p::aff-1*

Before injury

0 hr

3 hr

4 hr

B  **Primary fusion**

*aff-1/mln1; dpy-7p::aff-1*

Before injury

0 hr

2 hr

▲ Injury site   ⌐⎯⎯⌐ Menorah-menorah fusion

C

NS

\*   \*   NS   NS

**WT**   *aff-1(tm2214)*   *des-2p::aff-1;*
*aff-1(tm2214)/mln1*   *grd-10p::aff-1;*
*aff-1(tm2214)/mln1*   *dpy-7p::aff-1;*
*aff-1(tm2214)/mln1*

■ **1ry-1ry Fusion**   ■ **Menorah-Menorah Fusion**

■ **Menorah-Menorah Fusion &**
**1ry-1ry Fusion**   ■ **Degeneration**

1070
1071
1072
1073  **Figure 3-figure supplement 1.**
1074
1075  **Ectopic expression of hypodermal AFF-1 improves PVD regeneration in**
1076  **heterozygous animals**

40

1077
1078    **(A)** Regeneration by menorah-menorah fusion following PVD nanosurgery in *C. elegans aff-1(tm2214)/mln1; dpy-7p::aff-1* animals. PVD is shown before and after nanosurgery (T=0, 3, and 4 hr). PVD reconnection occurred through fused menorahs (pink bracket) and primary fusion did not occur (red arrowhead).
1082
1083    **(B)** Dendrite regeneration following PVD primary branch nanosurgery in *C. elegans aff-1(tm2214)/mln1; dpy-7p::aff-1* animals. PVD is shown before and after nanosurgery (T=0 and 2 hr). PVD reconnection occurred through primary fusion (blue arrowhead).
1087
1088    **(C)** Animals showing different PVD post injury consequences displayed in color coded pie graphs as Magenta- Menorah-Menorah fusion, Blue- primary-primary fusion, Magenta and Blue- Menorah-Menorah fusion and primary-primary fusion, Black-degeneration. Wild type n=22; *aff-1(tm2214)* n=32; *aff-1/mln1; des-2p::AFF-1* n=10, *aff-1(tm2214) /mln1; grd-10p::aff-1* n=11, *aff-1(tm2214)/mln1; dpy-7p::aff-*1 n=14. *P<0.05. P values for wild type and heterozygous genotypes are not significant (NS). Statistics was calculated using the Freeman-Halton extension of the Fisher exact probability test for a two-rows by four-columns contingency table, http://vassarstats.net/fisher2x4.html.
1097
1098    Dendrotomy site, red arrowhead; fused Menorah, pink bracket; primary fusion, blue arrowhead. Scale bars represent 20 μm.
1100

41

1101 **Supplemental movies legends**

1102

1103 **Movie 1. PVD dendrites touch and fuse following dendrotomy**

1104 Time lapse recording of an L4 wild-type animal just after injury. The z series images

1105 were recorded every 6 min, marker is *F49H12.4::GFP*. Arrows mark areas of fusing

1106 menorah tertiary branches. C marks PVD cell body.

1107 **Movie 2. A pseudo-colored presentation of depth information for Movie 1**

1108 Scale bar for the position in the z axis is shown at the bottom. The movie was

1109 obtained using the Zeiss LSM image browser DepthCod function.

1110 **Movie 3. Degeneration of the distal fragment following dendrotomy**

1111 Time lapse recording of a wild-type L4 animal after a two-photon injury. Posterior

1112 PVCR and PVCL are also marked with the *DES-2::GFP* marker and can be seen at

1113 the upper right corner. See **Figure 1G**.

1114 **Movie 4. Fusion and pruning during the PVD regeneration process**

1115 Intensity-values view of a time-lapse recording of an early L4 animal. Marker is

1116 *F49H12.4::GFP*. Menorahs from proximal and distal ends meet and fuse, bypassing

1117 the break induced by the two-photon injury. At the injury site growth and pruning of

1118 dendrites can be seen. Intensity scale bar is in **Figure 2D**.

1119 **Movie 5. AFF-1::GFP expression in PVD intact animals**

1120 Time lapse recording of *AFF-1::GFP* (cyan) expression inside and outside the seam

1121 cells (sc), and in the vulva (V) of an intact L4 animal shown in a two channels merged

1122 image. The z series images were recorded every 10 sec, PVD marker is

1123 *F49H12.4p::mCherry* (magenta). Arrows mark AFF-1 vesicles. See **Figure 4B**. The

1124 trajectory of vesicle 1 is shown in **Figure 4E**. Gut marks autofluorescent gut granules,

42

1125   easily distinguishable from AFF-1 vesicles in size, shape, and appearance in both

1126   channels.

1127   **Movie 6. AFF-1::GFP expression in PVD intact animals (zoom in of movie 5)**

1128   A magnification of a single *AFF-1::GFP* vesicle near the seam cells, ("vesicle 1").

1129   **Movie 7. AFF-1::GFP expression in PVD primary branch of injured animals**

1130   Time lapse recording of *AFF-1::GFP* expression (cyan) inside and outside the seam

1131   cells (sc), in the anchor cell (AC) and in the vulva (V) of a reconnected PVD L4

1132   animal after a two-photon injury anterior to PVD cell body. T=0 is 75 min after

1133   injury. The z series images were recorded every 20 sec, PVD marker is

1134   *F49H12.4p::mCherry* (magenta). Arrows point to vesicles containing AFF-1::GFP.

1135   **Movie 8. Magnification of Movie 7.**

1136   Magnification of an area with multiple vesicles, two are labeled (2,3). See **Figure 4**

1137   **D-E.**

1138   **Movie 9. AFF-1::GFP expression in PVD intact animal**

1139   Time lapse recording of *AFF-1::GFP* (cyan) expression inside and outside the seam

1140   cells (SC) of an intact L4 animal shown in a two channels merged image. The z series

1141   images were recorded every 10 sec, PVD marker is *F49H12.4p::mCherry* (magenta).

1142   Arrows mark AFF-1 vesicles.

1143   **Movies 10 and 11. AFF-1::GFP expression in a degraded PVD primary branch**

1144   **of injured animals**  Time lapse recording of *AFF-1::GFP* expression (cyan) inside

1145   and outside the seam cells (sc) of a reconnected PVD L4 animal after a two-photon

1146   injury anterior to PVD cell body, red arrowhead is the site of injury. T=0 is 75 min

1147   (movie10) and 150 min (movie 11) after injury. The z series images were recorded

1148   every 2 sec, PVD marker is *F49H12.4p::mCherry* (magenta). Arrows point to vesicles

1149   containing AFF-1::GFP.